Crack Growth Analysis of CNT Reinforced Polymer Nanocomposite using XFEM

A Dissertation submitted
in partial fulfilment of the requirements
for the degree of

Master of Engineering

in

CAD/CAM Engineering

by

Alok Negi

Registration No.: 801584002

Under the Supervision of

Dr. J.S. Saini
Associate Professor
Mechanical Engineering Department,
Thapar University, Patiala

Dr. Gagandeep Bhardwaj
Assistant Professor
Mechanical Engineering Department,
Thapar University, Patiala

MECHANICAL ENGINEERING DEPARTMENT
THAPAR UNIVERSITY, PATIALA

July, 2017

Certificate

This is to certify that the work done in the dissertation entitled **"Crack Growth Analysis of CNT Reinforced Polymer Nanocomposite using XFEM"** submitted by Mr. Alok Negi in partial fulfilment of requirements for the award of **Master of Engineering** degree in **CAD/CAM Engineering** at the **Mechanical Engineering Department** of **Thapar University, Patiala** is an authentic record of work carried out by me under the guidance of **Dr. J. S. Saini** and **Dr. Gagandeep Bhardwaj**. The matter embodied in this report has not been submitted in any part or full to any other university or institute for the award of any degree.

Alok Negi

Date: 14/07/2017
Place: Patiala

This is to certify that the above declaration made by the student concerned is correct to the best of my knowledge and belief.

Dr. J. S. Saini 14/7/17
Associate Professor,
Mechanical Engineering Department
Thapar University, Patiala

Dr. Gagandeep Bhardwaj
Assistant Professor,
Mechanical Engineering Department,
Thapar University, Patiala

Acknowledgements

I would like to express my sincere gratitude to my thesis advisors **Dr. Gagandeep Bhardwaj** and **Dr. J.S. Saini** for their continuous support, advice and guidance in the course of my research work. I would like to acknowledge and express gratitude to all the respected faculty members of Mechanical Engineering Department for their kind support and suggestions throughout my course work. I would also like to acknowledge my friends and colleagues who helped me throughout the duration of Master's program. I would to like to thank them for their fruitful inputs and discussions in the course of my research work. I was a great learning experience for me and I am hopeful, it will have a positive impact in my career.

At last, I would also like to express my love, affection and kindest regards to my parents and my sisters for their continuous support and encouragement throughout my life. I always admire them for their determination and sacrifices for my goals. It would not be possible without them.

Alok Negi

Abstract

In the present work, the crack growth analysis of carbon nanotube (CNT) reinforced polymer nanocomposite has been executed using extended finite element method (XFEM). The equivalent properties such as elastic modulus, Poisson's ratio, fracture energy and fracture toughness of the polymer nanocomposites have been evaluated by varying the percentage of CNT in terms of weight (both single walled CNT and multi walled CNT) in the polymer matrix. The elastic modulus of the polymer nanocomposite has been evaluated using modified Halpin-Tsai equation. The fracture energy of the polymer nanocomposite has been computed considering CNT pull-out and CNT debonding as the main toughening criterion.

In XFEM, the crack faces are modelled by discontinuous Heaviside jump functions, whereas the singularity in the stress field at the crack tip is modelled by crack tip enrichment functions. The value of stress intensity factor (SIF) is evaluated using domain form of interaction integral. The level set method has been used to track the crack growth. To obtain the crack growth direction, maximum principal stress criterion has been used in which the crack growth occurs in the direction perpendicular to the maximum principal stress. The numerical integration has been performed using Gaussian quadrature. In order to achieve higher accuracy in approximation of displacement and stress fields near the crack, sub-triangulation has been used in split and tip elements for the numerical integration. The numerical examples with an edge and a centre crack in the polymer nanocomposite are analysed and the influence of various parameters such as percentage of CNT and the aspect ratio on SIF are observed.

Keywords: Crack Growth, XFEM, Polymer Nanocomposites, CNTs, Halpin-Tsai, Edge crack, Centre crack, Stress intensity factor (SIF)

Table of contents

List of Figures

List of Tables

Nomenclature

C_h	Chiral vector
θ_c	Chiral angle
a_1, a_2	Unit vectors
E_{NT}	Elastic modulus of CNT
V_{NT}	Volume content of CNTs
V_m	Volume content of matrix
m_{NT}	Weight content of CNTs
l_{NT}	Length of CNT
t_{NT}	Thickness of CNT
d	Diameter of CNT
r_{NT}	Radius of CNT
ρ_c	Density of nanocomposite
ρ_m	Density of matrix
ϵ_{max}	Tensile failure strain of CNTs
l_{po}	Pull-out length of CNTs
τ_i	Interfacial shear strength
V_{fpo}	Volume content of pulled out CNTs
V_{fdb}	Volume content of debonded CNTs
l_c	Critical length of CNT
σ_{NT}	Strength of CNT
$\Delta G_{pull-out}$	Fracture energy associated with CNTs pull out
G_i	Interfacial fracture energy
ΔG_{db}	Interfacial debonding energy
$\Delta G_{rupture}$	Fracture energy associated with CNTs rupture
G_{CU}	Fracture energy of unmodified epoxy
G_C	Fracture energy of CNT reinforced nanocomposite
K	Stress intensity factor
G	Strain energy release rate
K_{IC}	Fracture toughness of nanocomposite
D	Elasticity tensor

∇	Gradient operator
n	Outward unit normal vector
ν	Poisson's ratio
K	Global stiffness matrix
u^h	Unknown displacement vector
u^H	Unknown displacement vector associated with crack split
u^{tip}	Unknown displacement vector associated with crack tip
f	External force vector
H	Heaviside function
x^*	Co-ordinates of discontinuity
F_b	Body force
B	Matrix of shape functions
q	Weighting function
$I^{(1,2)}$	Interaction integral
q	Weighting function
J	Jacobian matrix
$W^{(1,2)}$	Interaction strain energy
a	Crack length
L	Length of thin rectangular plate
B	Width of thin rectangular plate
K_I	Mode I stress intensity factor
K_{II}	Mode II stress intensity factor

Greek Symbols

ξ	Shape factor
Ω	Domain of concern
Γ_u	Displacement boundary
Γ_t	Traction boundary
Γ_c	Crack boundary
β_α	Crack-tip enrichment function
Ψ	Signed distance function
ψ	Normal level set function

φ	Tangential level set function
σ_{ij}	Stress tensor
ε_{ij}	Strain tensor
θ_C	Crack growth direction

Acronyms

FEM	Finite Element Method
XFEM	Extended Finite Element Method
CNT	Carbon Nanotube
SWCNT	Single walled Carbon Nanotube
MWCNT	Multi-walled Carbon Nanotube
CVD	Chemical Vapour Deposition
AFM	Atomic Force Microscopy
TOM	Transmission Optical Microscopy
LEFM	Linear Elastic Fracture Mechanics
DGEBA	Diglycidyl-Ether of Bisphenol A
TGDDM	Tetraglycidyl Diamino Diphenyl Methane
TGAP	Triglycidyl p-Amino Phenol
DGEBF	Diglycidyl Ether of Bisphenol F
ASFBP	Four Point Bend Specimen subjected to Anti-symmetric Loading
HT	Halpin-Tsai
FEG	Field Emission Gun
SEM	Scanning Electron Microscope
SIF	Stress Intensity Factor
CTOD	Crack Tip Opening Displacement

Chapter 1

Introduction

During the last few years, there has been an austere damage done to the environment due to global increase in industrial development and technology. Every day large number of products are being propelled in the global markets throughout the world for the public consumption purpose. Due to this massive demand of new varieties of products, the emphasis of the companies has been shifted more towards quantity rather than quality. This can have adverse impact on the environment due to huge volume of waste being engendered on the daily basis. Therefore it is important that the technology in future should be based on concepts such as minimum energy consumption, biological sustainability and sustainable raw materials. Thus the focus of research and development should be more toward development of high value and safer products. Among the different research fields, developing advanced nanocomposite materials is an important area of research because of the numerous advantages of nanocomposites over their counterparts. Nanocomposite materials are formed by a combination of two or more materials in which one of the constituents is having dimensions in Nano scale [1]. These multiphase materials consists a macroscopic continuous phase matrix reinforced with Nano fillers. The matrix phase and reinforcement phase are chemically different in nature usually separated by an interphase. Due to the high specific surface area of these Nano fillers, nanocomposites possess higher interface to volume ratio compared to conventionally used composites. At present, study of nanocomposites is an extensive area of research and polymer nanocomposites are a vital part of it.

Thermoset polymers, such as epoxy polymers are extensively used in numerous advanced composite research and adhesive applications due to their relative high specific modulus, specific strength, chemical resistance and thermal resistance [2]. However, due to their cross-linked arrangement, they display a brittle behaviour and are more prone to fracture. So to control this problem, one of the widely used technique is the addition of Nano fillers as the reinforcement phase in the polymer matrix to improve the physical properties of resulting thermosetting polymers. Various types of Nano fillers have been used in the past as the reinforcement which includes silica nanoparticles, nanoclays, carbon nanotubes and nanofibres, graphene, etc. [2]. Among the numerous varieties of reinforcements used in composite

applications, carbon nanotubes (CNTs) are one of the most widely used reinforcement phases due to their noteworthy properties. The carbon nanotubes (CNTs) were first reported by a Japanese scientist named Sumio Iijima while doing analysis of carbon clusters using Transmission Electron Microscopy [3]. CNT is a unique structural form of carbon having a cylindrical shape with a high aspect ratio. They can be categorized as a part of fullerene structural family [4]. Their distinctive tube-shaped structure is made by rolling graphene sheet which is a two dimensional honey-comb mesh arrangement in atomic scale [1]. CNTs have a superior mechanical, electrical and thermal properties which is the prominent reason behind their usage in a variety of applications as the reinforcement filler materials [5, 6]. They have wide applications in different fields such as aerospace and sporting materials, electronics, health and medicine, optics, material science, nanotechnology, etc. [1, 4, 7].

It has been well established that the reinforcement of carbon nanotubes in the polymer matrix improves the mechanical performance of the polymer nanocomposites with a significant improvement in their properties such as Young's modulus, tensile strength and fracture toughness. Tai *et al.* [8] studied the mechanical properties of phenolic composites using SWCNTs as reinforcements. Enhancement in tensile strength and elastic modulus of the modified epoxy polymer was reported. Gojny *et al.* [9] studied the influence of three types of CNTs on surface functionalization parameter and mechanical properties of an epoxy matrix. In the comparative study, SWCNTs, DWCNTs and MWCNTs were used as the reinforcements. Rise in stiffness, strength and fracture toughness of the epoxy polymer was reported, wherein the fracture toughness for 0.5 wt. % DWCNTs reinforced epoxy matrix augmented by about 43%. It was established by an additional study conducted by Gojny *et al.* [10] that with the use of MWCNTs as the reinforcement in epoxy matrix, there was an increment in thermal stability of the subsequent nanocomposite. Hsieh *et al.* [11] used MWCNTs as the reinforcement Nano fillers in their study. Fracture toughness under mode I loading and fatigue behaviour of a thermosetting epoxy polymer were observed with the help of a number of fracture toughness experiments. Results revealed an upsurge in elastic modulus (12% increase at 0.5 wt. % MWCNTs) and mode I fracture toughness of the thermosetting epoxy polymer. Moreover, enriched fatigue performance of the MWCNT reinforced nanocomposite was witnessed. Zhang *et al.* [12] examined the effects on fatigue behaviour of epoxy nanocomposites by the CNTs dimension and dispersion in epoxy matrix. It was established from the results that crack growth rates can be reduced by lessening the CNT diameter, increasing the CNT length and by enhancement in CNT dispersion. Tang *et al.* [13] investigated the fracture behaviour of epoxy reinforced with ozone functionalized MWCNTs. A surge in fracture energy of epoxy by 130 %

at 1 wt. % of CNTs in the epoxy matrix was reported. Ladani *et al.* [14] investigated the influence of aligned Nano fibres reinforcements on the properties of epoxy nanocomposites. The results revealed an upsurge in electrical conductivity (improvement by seven orders of magnitude up to 10^{-2} S/m) and fracture energy (improvement by 1600 %).

Fatigue plays a major role in premature failure of structural components. Under fatigue loading conditions, microscopic cracks within the material propagates at much higher speeds which can lead to unexpected failure. Thus, the structural components are expected to be reliable under fatigue loading situations, especially in presence of any internal or external defect. As traditional strength based theories does not take the effect of defects, discontinuities or irregularities into account, developed either at the production stage or in the course of load application, fracture based numerical simulations provide a broad application in estimation of component life expectancy. Since, CNT reinforced polymer nanocomposites possess desirable mechanical properties for being used as in a variety of structural applications, analysis of static and propagating cracks in polymer nanocomposites using numerical simulation techniques is an important area of study. A number of methods such as element free Galerkin method [15], reproducing kernal particle method [16], meshless local petrov Galerkin method [17], extended finite element method [18] and isogeometric analysis [19] are available to simulate the cracked structures.

The extended finite element method (XFEM) is an extended version of standard finite element method (FEM). It is a popular numerical technique in modelling crack propagation that does not require a remeshing process. In the framework of finite element method, a conformal mesh is a necessity besides the use of special elements to handle asymptotic stresses near the crack tip domain [20]. In comparison to FEM, the XFEM is based on the concept of partition of unity in which a discontinuity/crack can be modelled independent of the finite element mesh. In XFEM, the standard finite element approximation is enriched locally with the aid of certain additional functions. The level set method originally proposed by Osher and Sethian [21] is efficient for the tracking of discontinuity. The first application of level set method to XFEM was done by Stolarska *et al.* [22], and Sukumar *et al.* [23]. Daux *et al.* [24] successfully applied XFEM to model a set of discontinuities which included cracks with multiple branches and intersections, holes, and cracks evolving out from holes. Sukumar and Prevost [25] carried out the computerized implementation of XFEM for the quasi-static crack growth analysis in isotropic and bi-material media. Wyart *et al.* [26] applied XFEM to simulate three-dimensional crack growth problems within the framework of commercial finite element codes. The three-dimensional problem with a crack domain was sub-structured into two parts *i.e.* safe domain

which was simulated by a commercial finite element code and a cracked domain simulated by XFEM.

1.1 Carbon Nanotubes

Carbon Nanotubes (CNTs) are a unique structural forms of carbon which forms the part of fullerene group. From the definition viewpoint, a CNT is a hollow cylindrical nanostructure with the walls formed by atomic layer of carbon, known as graphene. Graphene is a hexagonal structure of carbon atoms which are covalently to each other. CNTs can be distinguished from the rest of carbon allotropes with the help to their unique structure, dimensions and defects. CNTs have extraordinary mechanical properties, electrical and thermal properties which can be made into use in several applications. From the mechanical properties viewpoint, CNTs exhibit an extraordinary elastic modulus of around 1 TPa [27]. The tensile strengths of CNTs varies from 11 to 63 GPa based on the number of reports by researchers during the last decades [6]. Their diameter varies from 1 nm to values in hundreds nanometres [28]. Similarly, they normally have lengths in micrometres, millimetres and even centimetres [29]. CNTs can have density lower up to a value of 1.3 g/cm^3 [27]. For the production of these amazing cylindrical structures *i.e.* SWCNTs and MWCNTs for numerous applications, generally used methods includes arc-discharge technique, gas-phase catalytic-growth via carbon monoxide, laser ablation method and chemical vapour deposition technique (CVD) [28].

Based on the hollow cylindrical structure of CNTs, they can be classified into two basic types

i. Single-walled Carbon Nanotube (SWCNT): Single-walled Carbon Nanotube (SWCNT) is formed by the use of a singular graphene sheet wrapped up to form a tube [30, 31]. They have diameter in range of nanometres. The carbon atoms in the cylindrical structure of SWCNT have a fractional sp^3-character that rises as their radius of curvature decreases. They have unique electrical properties and shows extraordinary mechanical performance projected from theoretical modelling as well as experimental results. Figure 1.1 (a) shows the basic structure of SWCNT.

ii. Multi-walled Carbon Nanotube (MWCNT): Multi-walled Carbon Nanotube (MWCNT) comprises of an array of nested graphene tubes arranged concentrically with interlayer separations of about 0.34 nm [28]. They are having diameter in the range of 2 to hundreds of nanometres and lengths in the range of microns to millimetres or sometimes even centimetres. Double-walled Carbon Nanotubes (DWCNTs) are a special case of MWCNTs that consist of two concentric graphene cylinders. They exhibit higher flexural modulus as

compared to SWCNTs due to two walls and better toughness values to that of MWCNTs because of smaller size [32]. Figure 1.1 (b) shows the basic structure of MWCNT.

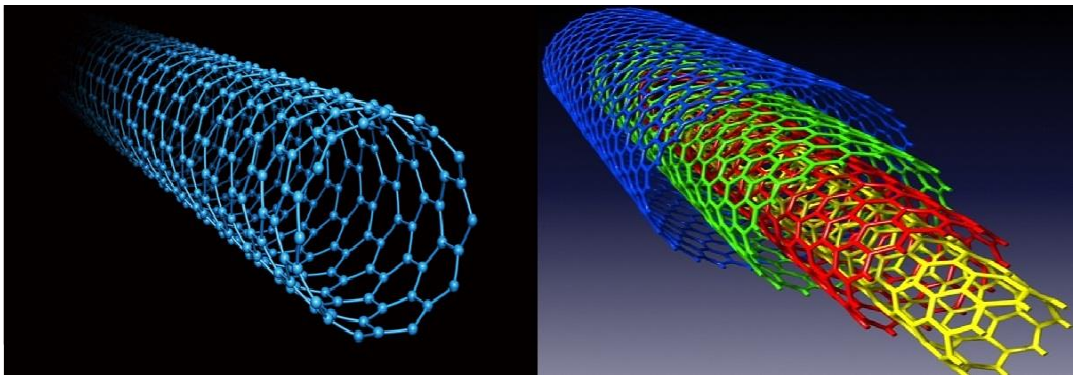

(a) (b)

Figure 1.1: Basic structures of (a) SWCNT, (b) MWCNT [W1, W2]

1.2 Geometric Structure of CNTs

The geometric structure of CNTs is similar to that of carbon fibres. Based on the early study of CNT structure using Transmission Electron Microscopy (TEM) and Scanning Tunnelling Microscopy (STM) techniques, CNTs can be defined as seamless and rolled-up graphene cylinders with constant radius comprising a hexagonal network of carbon atoms [33]. This benzene type hexagonal set-up recurs periodically, as each carbon atom is bonded strongly by covalent linkages to the three adjacent atoms. The atomic structure of CNTs depends upon its chirality unique to each and every nanotube. Chirality of CNTs is defined by the packing of carbon hexagons in the graphene sheets and represented by a chiral vector (C_h) and chiral angle (θ_c) [34]. The indices of the chiral vectors indicate the morphology of CNTs and change in morphology alters the nanotube properties. The chiral vector [34] can be described with the help of equation (2.1).

$$C_h = na_1 + ma_2 \tag{2.1}$$

where, the variables n, m represents the number of steps alongside the carbon bonds of the hexagonal lattice; and a_1, a_2 represents the unit vectors, as shown in Figure 1.2. There are three distinctive structures of CNTs based on their chirality *i.e.* zig-zag $(n, 0)$, armchair (n, n) and chiral (n, m) where the value of n is greater than m. The work of the chiral angle is to determine the extent of twist in the tubular structure of CNT. Depending upon the chiral angle values of 0^o and 30^o, two restricting cases comes into existence based on the geometric structure of carbon atoms in CNT *i.e.* ziz-zag (0^o chiral angle) and armchair (30^o chiral angle). In case of chiral arrangement of CNT, the value of the chiral angle varies from 0^o to 30^o. In the zig-zag structure of CNT, hexagonal arrangement of carbon atoms forms a zig-zag configuration

alongside the circumference of CNTs. In armchair structure, hexagonal lattice is rotated by 90° with regard to zig-zag pattern. Figure 1.3 illustrates the rolling operation and three different geometric structures of CNT obtained by rolling the graphene sheet.

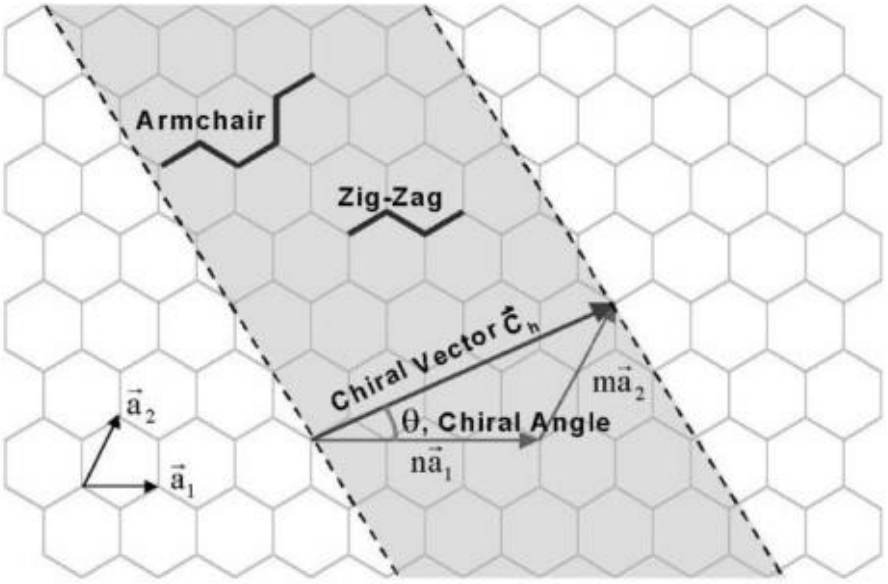

Figure 1.2: Schematic diagram showing the formation of carbon nanotube from hexagonal sheet of graphene [35]

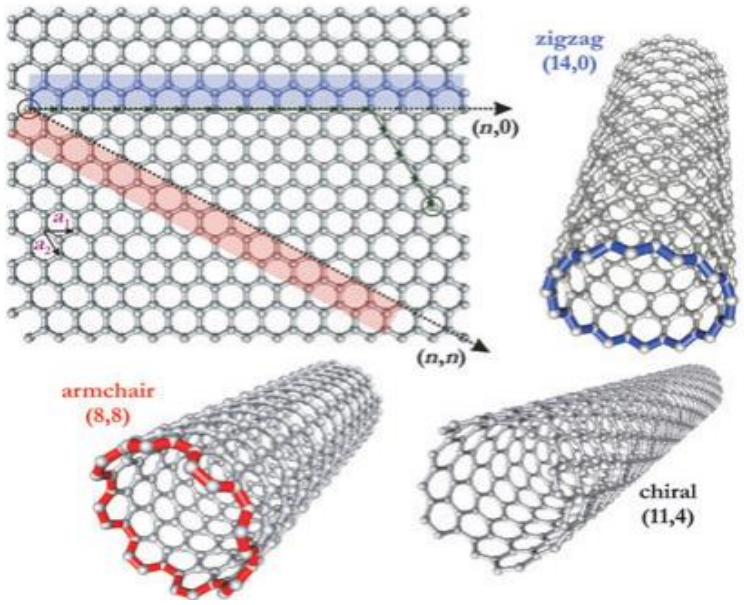

Figure 1.3: Rolling operation and different geometric structures of CNTs [36]

1.3 Properties of CNTs

The exceptional mechanical, electrical and thermal properties of CNTs can be utilized in a wide range of applications. CNTs mechanical properties can be extremely useful in advanced composites relating to structural applications. Similarly, good electrical and thermal properties

of CNTs owing to their unique geometrical shape can also be successfully utilized in thermal and electrical applications.

1.3.1 Mechanical Properties

The in-plane modulus of graphite sheet is 1.06 TPa [37]. The tensile strength of graphite has been estimated to be 130 GPa on the basis of properties of carbon bonding [37]. Due to these extraordinary properties of graphite, it was expected from carbon nanotubes to have high strength and stiffness. Earlier researches regarding the mechanical properties of CNTs were mainly based on computer simulation. The first measurements to be done mechanically were conducted on MWCNTs prepared by the arc discharge technique. For the MWCNTs measurements, Treacy *et al.* [38] used thermally induced vibrations with the aid of TEM. A high elastic modulus varying from 0.41 to 4.15 TPa was observed. Afterwards, elastic modulus values ranging from 0.7 TPa to 1.3 TPa were reported by Poncharal *et al.* [39] by inducing electro-mechanical resonant vibrations. Wong *et al.* [27] studied the mechanical properties MWCNTS using AFM. MWCNTs were held to one of the end of molybdenum disulphide surface and an average value of 1.28 TPa for the elastic modulus was observed. During the strength measurements, a value of 14 GPa was obtained as the average bending strength. Salvetat *et al.* [40] using AFM for the measurement of arc discharge MWCNTs obtainined an elastic-modulus value of 810 GPa. Yu *et al.* [6] studied the mechanical properties of MWCNTs using tensile loading experiments for individual MWCNT. The length of MWCNTs in the experimental study varied from 1.8 μm to 11 μm, with the number the tubes ranging from 2 to 20. A maximum tensile strength of 63 GPa was attained corresponding to MWCNT having an outer diameter of 20 nm, whereas the strengths ranged between 20 to 63 GPa. Behabtu *et al.* [41] reported an average value of 1.0 ± 0.2 GPa and 120 ± 50 GPa for tensile strength and elastic modulus of CNTs.

The first-time measurements of mechanical properties of SWCNTs were done by Salvetat *et al.* [42] by means of AFM technique, in which SWCNTs attained the exceptional elastic-modulus value of 1 TPa. Yu *et al.* [43] measured the mechanical properties of SWCNTs ropes making use of SEM. Measurement was conducted for SWCNT bundles prepared by laser abrasion technique. A high elastic modulus values ranging between 0.32 to 1.47 TPa was obtained, with the highest value corresponding to CNT bundle of 35 nm diameter. Similarly, the tensile strengths showed exceptional values ranging from 10 and 52 GPa, with the highest value corresponding of CNT bundle of 40 nm diameter. The maximum strain value of 5.3 % was attained for SWCNT bundle corresponding to 23 nm diameter. The most commonly used

production method for MWCNTs is CVD. Though CNTs made using this method generally have a large number of defects, due to which their physical properties of CNTs get suffered. However, this process is significant since with the utility of this method, CNTs can be manufactured in very large quantities, with a relative low-cost. The first measurements on CVD produced MWCNTs were done by Salvetat *et al.* [40] in which elastic modulus values ranged between 12 to 50 GPa. Figure 1.4 shows the tensile strength comparison of commonly used popular engineering materials in engineering practises.

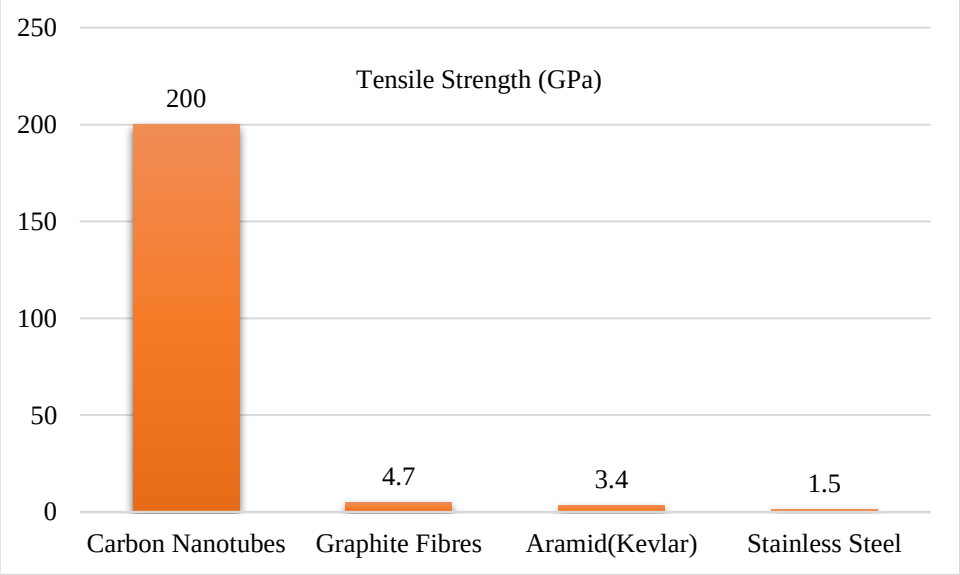

Figure 1.4: Comparison study of popularly used engineering materials [44]

1.3.2 Electrical Properties

High value of electrical conductivities in CNTs forms a part of excellent properties of CNTs. These high values have drawn interest of many researchers from time to time. Normally, in case of CNTs, the electrical properties are dependent on their unique geometric nanostructure and are found to be a function of their chirality *i.e.* the way in which the hexagons are oriented along the axis. Apart from the chirality, electrical properties are also dependent on the degree-of-twist along with the diameter of CNT. Thus, depending on the geometric structure, CNTs can behave as metallic or semi-conducting. Armchair CNTs are always semi-metallic. Zig-zag and chiral CNTs properties may vary from semi-metals to large band gap semiconductors. CNTs have an exceedingly wide range of conductivities, reported by a number of researchers varying between 10 S cm^{-1} to 67000 S cm^{-1} [35, 45]. This wide variation is due to many factors, in which defects involved with CNTs are of major concern. Behabtu *et al.* [41] reported high values for electrical conductivities of CNTs, when measurement was done at room temperature with an average

value of 2.9 ± 0.3 MS/m. Furthermore, with the doping of iodine, the electrical conductivity raised to value of 5 ± 0.5 MS/m.

1.3.3 Thermal Properties

The thermal properties of CNTs haven't received much attention by researches due to difficulties which are generally observed while processing better quality CNTs. In case of CNTs, their geometric structure directly influences their thermal behaviour. CNTs exhibit a unique property which is termed as ballistic conduction. According to it, CNTs exhibit superior thermal conduction along their length while exhibiting an excellent insulation in the lateral direction. An average thermal conductivity value of 380 ± 15 W/mK was reported for CNTs having a length in the range of 1 mm, which was doubled by the doping of iodine [41]. The thermal properties of CNTs are affected adversely by the crystallographic defects associated with them. These defects results in the photon scattering in structure of CNTs which in turn reduces the thermal conductivity of CNTs. More number of theoretical and experimental studies are needed to fully understand the thermal properties to CNTs.

1.4 Matrix

Matrix can be defined as a continuous phase in which Nano fillers are added as a primary or secondary reinforcements. While fabricating nanocomposites, matrix serves the two important purposes *i.e.,* (i) Protecting the reinforcement phases from environment by binding them together in a place and (ii) Suitable stress distribution between the constituent phases by getting self-deformed under an action of an external load [46]. Matrix may be subjected to temperature variations, electricity conduction, moisture sensitivity etc. depending upon the type of application. Some of the major functions of matrix are:

i. Holding the reinforcements fillers together.
ii. Protecting the reinforcement fillers from external surroundings.
iii. Distributing the loads evenly between reinforcement fillers so that all reinforcement fillers are subjected to the same amount of strain.
iv. Enhancing the properties of nanocomposite in transverse direction.
v. Improving the impact and fracture resistance of a nanocomposite.
vi. Crack arresting by providing alternative failure paths along the interface between the reinforcement filler and the matrix.
vii. Providing better finish to the final product.

Some of the properties that are expected from matrix are:

i. Lower moisture absorption.
ii. Low value of shrinkage.
iii. Good elasticity.
iv. Low value of coefficient of thermal expansion.
v. Better flow characteristics.
vi. Reasonable strength, modulus and elongation.
vii. Good strength at higher temperature.
viii. Good performance at lower temperature.
ix. Excellent chemical resistance.

A composite can also be classified based on the type of matrix materials. Some of the generally used matrices are

1. Polymer matrix
2. Metal matrix
3. Ceramic matrix
4. Carbon and graphite matrix

1.4.1 Polymer Matrix

Polymers serves as an ideal matrix material as they can be processed easily, have lower density, are lightweight and generally have curing temperature is in the lower range in comparison to majority of the materials [47]. Moreover, almost every type of reinforcement *i.e.* inorganic or organic can be used with polymer matrix. Due to these certain advantages of polymer matrix, manufacturing costs are on the lower side while dealing with reinforced plastics or polymer nanocomposites. Polymers are generally categorized into two main types on the basis of their unique properties *i.e.* thermoplastics and thermosets. Polyethylene, polystyrene, polyamides, nylons and polypropylene comes under the category of thermoplastics. Whereas epoxy, phenolic polyamide resins, polyester comes under the category of thermosets.

Thermoplastics: Although thermosets are more popular as compared to thermoplastics due to their properties, thermoplastics are also finding a lot of applications and the interest in them has increased considerably in present years with the growth of high performance thermoplastics. Thermoplastics possess a one or two-dimensional molecular arrangement and the major advantage with them is that they can be repeatedly formed by heat and pressure [46]. They habitually have a molecular weight in the upper range in comparison their counterparts. In thermoplastics polymer, the molecular chains are associated together with the help of intermolecular forces which can be weakened by increasing the temperature. They can be

softened by increasing the temperature above the glass transition temperature and can be strengthened by dropping the temperature. In case of lowering the temperature, a number of new secondary bonds are formed and the polymer generally reverts back to its original structure. Due to this behaviour of thermoplastic polymer, they can be used and recast again, thus reducing the material wastage. Their performance is thermally steady at high temperature and have a high glass transition temperature. They generally attain higher glass transition temperature due to their stiffness, linear chains and high molecular weight. They also have higher stiffness and thus exhibit good creep resistant properties. Moreover, they are relatively tougher and less sensitive to moisture.

Thermoset: Thermosetting resin can be described as a low molecular weight pre-polymer generally having a viscous nature. Thermosetting resins in contrast to thermoplastics, undergo a permanent polymerization process. After curing, thermosetting resins generates a well bonded three dimensional structure which is termed as a thermoset or a thermosetting polymer. Thermoset polymers suffers everlasting plastic deformation under an action of load and they normally decompose before melting. When thermosets are used as the bulk material, they are denoted as the thermoset polymer matrix. Thermosets have higher strength in comparison to thermoplastic polymer. They are also more suitable at high temperature applications due to their ability to preserve their three dimensional arrangement till the decomposition temperature. In case of thermosets, robust covalent bonding acts amongst the polymer chains and thus cannot be easily broken. Epoxy, polyester and phenolic resins are the most frequently used thermoset polymer, amid which polyester resins are extensively used in several common engineering goods and composite applications. Phenolic resins are affluent in carbon and have decent thermal properties. They are routinely used in high temperature applications as an ablative material in thermal shield systems. However, among the various types of thermosets available in the market, epoxy resins are the most widely used group of thermoset resins. They are largely used as adhesives, owing to their high stiffness and strength values. Increasing the toughness of epoxy by reducing its brittle behaviour has been the subject of many researches since long.

Epoxy resins which are also termed as poly-epoxides, generally forms a class of sensitive pre-polymers that contains two or more epoxide groups prior to cross-linking operation. Epoxy resins in broad-spectrum own good thermo-mechanical, electrical and chemical resistant properties [46]. Epoxy resins have been successfully utilized in composite applications since 1960s. In case of epoxy resins, cross linking happens through catalytic homo-polymerisation, or with a widespread range of co-reactants embracing poly-functional amines, acids, phenols and alcohols. The cross networking technique is recognized as the curing practise

and the co-reactants are labelled as the hardeners. Epoxy resins after the curing process forms a thermosetting polymer with better mechanical properties, thermal and chemical resistance. They have an extensive range of commercial applications which includes their use as high performance industrial adhesives, construction materials, protective coatings, textile finishing, tooling, moulding, casting and automobile applications [48]. Dry epoxy resin systems are utilized in aircraft fabrication and marine engineering applications by substituting polyesters in specialized operations where under-water strength is of higher concern. But despite the numerous benefits of epoxy resins *e.g.* commendable mechanical properties and thermal stability, epoxy resins are brittle in behaviour due to their higher crosslink density [46, 47, 49]. The lower toughness behaviour of epoxy resins is one of the key drawback that prevents its usage across several applications. So, it is imperative to overcome this deficiency, and the best methodology for increasing the fracture toughness is to supplement a second phase in the epoxy matrix acknowledged as nanoparticles, which activates in the course of curing treatment procedure. These Nano fillers activates toughening mechanisms in crack propagation as they demonstrates high specific strength-to-weight ratios, lower densities, higher stiffness and higher toughness values. The crucial objective to reinforce epoxies using a range of Nano fillers is to permit the desired properties to be tailor-made agreeing to the engineering requirements while keeping the cost in the lower end.

Various researchers have started to improve the performance of epoxy by adding additives for either biodegradation or performance enhancement which ultimately leads towards a larger life span of the material. These upgraded properties of the epoxy are then used the modelling parameter for the design simulations. The level of adhesion in epoxy resins forms important area of concern while selecting polymer matrix for CNT reinforcement. Since, epoxy resins possess good thermal and mechanical properties, have higher chemical and corrosion resistance and forms sturdy bonds with virtually entirely all surfaces excluding a few non-polar substrates, they form an appropriate matrix base for CNT dispersion with greater adhesion capabilities. In addition to admirable properties of the epoxy resins, they have number of sustainable characteristics associated with them which emboldens their usage for the production of nanocomposites for advance applications. From the sustainability point of view, epoxies on curing do not cause volatile emissions in spite of the presence of volatile solvent in it. Epoxy resins can be also used to form lightweight constructions with commendable insulation properties, which is one of the remarkable aspect of epoxies from the sustainability standpoint. Reducing weight of composite by specialised design improves environmental management by reducing material consumption that ultimately be landfilled or recycled. Though technology for

recovering epoxy resin from its processed composite state is in its premature stage, studies suggest that recovery is achievable through gasification and a few more processes. The most familiar epoxy is the alpha-epoxy which comprises a three member ring arrangement [50]. It is commonly cured in temperature range of 5 to 150°C via amine hardener. The most commonly used epoxy resins, which are at present are being used in a majority of applications are DGEBA, TGAP, TGDDM and DGEBF. In the present work, Diglycidyl ether of bisphenol-A (DGEBA) resin having an equivalent epoxy weight (EEW) of 186 is considered as the matrix base [11]. DGEBA is the first commercially used epoxy resin and has a wide application in composite field.

1.5 Extended Finite Element Method

Finite Element Method (FEM) is a powerful numerical tool that is used to solve a wide range of engineering and physics problems. The reason for the development of FEM was the wide range of complexities involved in obtaining the exact mathematical solutions to problems involving complex geometries, loadings and material parameters. Due to such issues, the research scenario shifted more towards the use of numerical methods to obtained approximate solutions to problems of complicated nature. In FEM, instead of solving the governing differential equations using lengthy mathematical approach, equations are converted to linear set of algebraic equations which are relatively easy to solve. The domain under consideration is divided into smaller parts or more specifically finite elements, which are interconnected to one another with the help of nodes. After this step, equations are formulated for each finite element, which are then combined afterwards to obtain solutions for the overall domain. From the structural analysis point of view, the unknown displacements, stresses and strains are computed every node of the finite element mesh.

Over the last few decades, a lot of work has been done in the field of FEM. A large number of FEM software packages have been developed for solving a wide range of engineering problems. One of many applications of FEM is the analysis of crack growth in structures involving defects in the form of some irregularities or discontinuities in the geometry of structure. In such situations, FEM provide a broad application in estimating a component life expectancy. In the present context, FEM can be helpful in predicting the life of the polymer nanocomposites in presence of internal or external defects. Though FEM can be successfully used to model crack growth problems, there are some drawbacks in FEM. One of the major drawback in FEM is re-meshing which is essential after each step, in case of crack growth problems. FEM necessitates the crack face to align with the edges of the finite elements. As a

consequence, there is a necessity of conformal mesh in FEM, with an additional requirement of special elements to handle crack tip asymptotic stresses. In this way, FEM can be very cumbersome and time consuming in nature. This drawback of FEM lead to the development of extended finite element method (XFEM). XFEM is an effective numerical tool for simulating crack growth in materials subjected to external cyclic loading. In XFEM, a crack is modelled independent of the finite element mesh avoiding the requirement of re-meshing. The standard finite element approximation in XFEM is enriched locally with the aid of some supplementary enrichment functions, which are obtained from the theoretical context of fracture mechanics.

1.5.1 Fracture Mechanics

Fracture mechanics is a subject of study where the materials tolerance to fracture is characterized. The study in fracture mechanics is concerned with the driving forces on the crack which might create suitable situations for crack growth. A crack can be defined as a sharp void or discontinuity in the material that acts as a stress amplifier. Traditionally, a material is supposed to have failed when the maximum tensile stress/strain value in the structure exceeds a certain threshold value. The effect of cracks or crack like defects on the strength is not taken into consideration. This sometimes leads to very high predicted strength in contradiction with the actual strength of the material. Many structural failures could not be explained by the traditional strength based approach. Most prominent among them was the failure of Liberty ships during World War II. These instances of catastrophic failures triggered the development of fracture mechanics. It was already known that every structure has flaws or cracks inside it. Whether these cracks or flaws will grow or not depends not only on the applied loads but also on the size of the existing cracks or flaws. Taking these factors into consideration, two important material parameters were developed *i.e.* energy release rate and stress intensity factor. These parameters are important in brittle and less ductile situations. Brittle fracture is characterized by fast crack growth with low energy dissipation, often leading to failure of components in a short duration of time. In brittle fracture phenomenon, crack velocity is reasonably high with very slight micro deformation. Conversely, ductile fracture takes place with some amount of stable crack growth before the final failure. Ductile fracture is characterized by high energy dissipation and involves significant plastic deformation before the crack instability occurs.

Linear elastic fracture mechanics (LEFM) is the fundamental theory of fracture mechanics which was established on the assumption material behaves in a linear elastic manner. Fracture mechanics find its roots in the work done by Inglis [51] which was to quantify stress

concentration near a hole or a notch depending on the radius of curvature of the notch. The problem of higher magnitude of stress near a discontinuity was resolved by Griffith [52] who provided the energy based concept of crack growth and provided the term energy release rate. The work done by Griffith was then improved by Irwin [53] who gave the stress based criteria of crack growth. It is a basic and simplified theory which deals with sharp cracks in elastic materials. The stress field in the proximity of the crack tip is assessed by the theoretical background of theory of elasticity. LEFM predicts infinite stress at the crack tip which is physically impossible. In any structure/component under the applied load, the stresses developed around the crack tip are quite high. These stresses are responsible for the development of an inelastic region nearby the crack tip. In general, the inelastic zone size is quite small in comparison to other linear dimensions of the structures. LEFM theory can be applied as long as the inelastic zone near the crack tip is very small. In case of ductile materials having a large plastic deformation near the crack tip, concepts such of J-integral and Crack Tip Opening Displacement (CTOD) were developed which helped in characterizing the crack.

1.6 Report structure

In the present work, XFEM has been used to analyse the effect of cyclic loading on a thin plate structure. The thin plate is made up of CNT reinforced polymer nanocomposite material and is subjected to cyclic loading under different crack conditions. Level set method has been used to track the discontinuity. The crack face has been modelled using Heaviside step function to reduce the computational complexity and for the crack tip, crack tip enrichment functions have been used. The direction of crack growth has been estimated using maximum principal stress criterion. The value of stress Intensity Factors (SIFs) have been computed using domain based interaction integral approach. The equivalent properties of the CNT reinforced polymer nanocomposite have been computed using both single walled carbon nanotube (SWCNT) and multi-walled carbon nanotube (MWCNT) as the reinforcement in the polymer matrix. The dissertation includes the following chapters.

Chapter 1 provides a brief introduction to thesis topic highlighting its importance. This chapter presents the background of the thesis which comprises information regarding carbon nanotubes, matrix and extended finite element method.

Chapter 2 provides the literature review of the thesis work. This chapter presents the influence of parameters such as carbon nanotubes alignment, dispersion and functionalization on the mechanical performance of the subsequent nanocomposite. Various toughening and fracture

mechanisms of polymer nanocomposites forms have been explained based on the literature review.

Chapter 3 deals with the detailed mathematical modelling of the problem which provides the theoretical background to evaluate the equivalent properties of the subsequent nanocomposite such as elastic modulus, Poisson's ratio, fracture energy and fracture toughness. This chapter provides a detailed introduction to extended finite element method which includes mathematical formulation required to conduct crack growth simulation.

Chapter 4 provides the results and discussions based on the problems under consideration. This chapter presents the effect of different parameters on the equivalent properties of the subsequent nanocomposite. Further, this chapter presents the results of the crack growth simulations conducted on a thin rectangular plate containing an edge crack and a centre crack.

Chapter 5 provides the conclusions of the thesis work and presents its future scope.

Chapter 2

Literature Review

Since the discovery of CNTs, there has been a lot of applications of CNTs in different fields of research and technology. One of these areas is the development of advanced nanocomposites using CNTs as the reinforcement. Today, it is an important area of research because nanocomposite have a great potential in applications where strength and weight of the component matters a lot. Moreover, nanocomposites can be more advantageous as compared to conventional micro-composites as their properties can be enhanced with the limited amount of reinforcement. They are a set of highly promising composite materials with a wide range of applications in a number of research areas such as automotive, aerospace, defence and energy sectors. Some of their applications include their use as aerospace structural panels, ultra-light-weight space structures, high performance sporting equipment's and space mirror substrates [7]. Their use as automobile bumpers is among the newer set of their applications. Generally, bumpers used in automobiles are required have a lower weight with better mechanical properties. These conditions can be easily fulfilled by CNT reinforced nanocomposite properties when comparing to presently used fiberglass bumpers at a relatively low CNT content. Apart from the structural applications, CNT modified nanocomposites can also be used in electrical, optical and thermal applications.

A number of experimental and simulation results based on the improved mechanical properties of CNT reinforced polymer nanocomposites have been reported by various researchers from time to time, since its emergence. So based on the literature survey, various issues regarding CNT reinforced polymer nanocomposite came into picture. One such issue is that whether the superior mechanical properties of the CNT will be effectively utilized when the nanocomposite is under application. Another issue that came into picture is that whether the high surface area of CNTs will promote adequate interactions for an effective load transfer between the matrix phase and the CNTs. And lastly, how the chemical bonds between CNT and matrix can improve the mechanical properties of the nanocomposite. This issue is related to adhesion level at the CNT/matrix interphase. These issues can be successfully tackled with by adjusting a set of parameters which can affect the mechanical properties of the resulting nanocomposite. CNTs dispersion, alignment and functionalization are some of the important parameters that influence the subsequent properties of a nanocomposite.

2.1 Dispersion and Alignment

Dispersion is one of the most fundamental matter while dealing with CNT reinforced nanocomposites and plays a crucial role in refining the mechanical properties. CNTs usually have a great surface area which can be efficiently exploited by appropriate dispersion of CNTs and thus attaining a suitable interfacial bond between CNTs and the polymer molecules. However the weak forces (van der-Waal interactions) that exists between clusters of CNTs present in resin system, often leads to agglomeration which is one of the biggest challenge while dealing with CNTs. Due to this problem, only few molecules of the polymer penetrate among the CNTs and react with them during the mixing process. Agglomeration can also result in initiation of cracks within the matrix during the load transfer operation. Thus, in order to achieve an effective reinforcement of CNTs within the resin system, CNTs should be dispersed in a uniform fashion within the polymer matrix. This is important in order to achieve much more effective load transfer from the matrix molecules to the CNT network. Moreover, it outcomes in uniform stress distribution and curtails the presence of stress concentration regions in the material.

Poor dispersion has negative effects in many situations, often leading to reduction in strength and modulus of the resulting composite [54]. This happens when the content of CNT is increased beyond a certain limit at which aggregation starts to take place. SWCNTs forms bundles more easily in contrast to MWCNTs due to relative lower dimensions. As a result, dispersion of SWCNTs require more expertise in comparison to MWCNTs. There are many physical blending techniques that can be used used for the effective mixing of CNTs within the matrix system such as ultrasonic mixing, high energy sonication, melt processing, calandering, electro-spinning, etc. [1]. Moreover, for the enhancement of dispersion process, other techniques such as chemical functionalization and in-situ polymerization can also be used [55].

Thostenson and Chou [56] studied the influence of variation in dispersion parameters on the final fracture toughness of the MWCNTs reinforced resin. The MWCNTs used for study were prepared by CVD technique. For the effective dispersion of MWCNTs in the epoxy resin, calendaring approach was utilized with the variation in gap settings between the rollers of three roll mill. It was witnessed that different gap settings lead to different agglomeration of MWCNTs within the epoxy resin system. Fracture toughness tests were conducted using single-edge notch bending technique. At a relative low % by weight content of MWCNTs inside the epoxy system, improvement in fracture toughness of the resulting nanocomposite was reported. Interfacial debonding and pull-out of MWCNTs were observed to be the main toughening

mechanisms resulting in improvement of fracture toughness. Figure 2.1 presents the outcomes of the fracture toughness measurements. For those modified resins where the gap setting between the rollers of the three-roll mill was larger (10 µm), the overall fracture toughness was higher in comparison to those with smaller gap (5 µm). Besides the improvement in fracture toughness values, increase in thermal conductivity of the MWCNTs modified epoxy system was observed by around 60 % at 5 % by weight content of MWCNTs in comparison to that of pristine epoxy system.

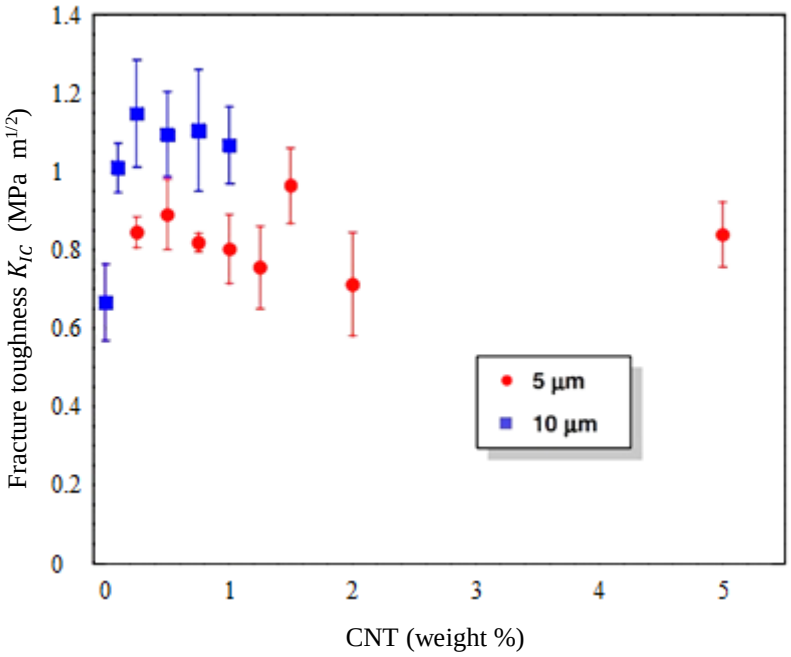

Figure 2.1: Fracture toughness results [56]

Song and Youn [57] studied the effect of poor and well dispersion of CNTs on the different properties of epoxy nanocomposites. SEM and TEM were used to characterize the dispersion process in the nanocomposite. Improvement in the physical properties of epoxy nanocomposite was observed with increase in CNT content within the epoxy matrix. For the dispersion process, ethanol was used as the solvent. Three different % by weight content of CNT were used for the reinforcement in the epoxy matrix *i.e.* 0.5 %, 1.0 % and 1.5 %. The CNTs were agglomerated due to poor dispersion which was not the case with the well dispersed CNTs. Improvement in the tensile strength was witnessed, when the CNT were well dispersed with the epoxy matrix. A higher reduction in fracture strain was witnessed for poorly dispersed CNT modified nanocomposite in comparison to well dispersed CNT modified nanocomposite. Apart from the mechanical properties, electrical and thermal properties were found to be improved for the epoxy nanocomposite with well dispersed CNTs.

Aligning CNTs within the matrix system is of less significance in comparison to dispersion. While aligning of CNTs is generally necessary for the improvement of strength and stiffness of the subsequent nanocomposite, it is not always favourable. The anisotropic behaviour of the aligned nancomposites due to CNT alignment along a particular direction, must be avoided in bulk samples. However, in the case of fibres, alignment has no drawbacks and is a decent way to take full advantage of reinforcement. Additionally, CNTs alignment permits a superior load transfer, electrical and thermal properties along a certain direction. Research studies have also shown that by aligning CNTs perpendicular to the crack front, crack bridging can be contained. There are a number of methods that can be used for the effective alignment of CNTs within the polymer matrix. These methods include ex-situ alignment, filtration, plasma-enhanced chemical vapour deposition, force-field induced alignment, magnetic field-induced alignment, electro-spinning induced alignment and liquid crystalline phase-induced alignment of CNTs.

Khan *et al.* [58] studied the effect of CNTs alignment on the properties of CNTs modified epoxy nanocomposite for both aligned and random orientation of CNTs in the epoxy system. In the results, much enhanced electrical conductivity was witnessed due the improved alignment of CNTs. Different properties of modified epoxy nanocomposite such as elastic modulus and fracture toughness also got improved in comparison to nanocomposite containing randomly oriented CNTs in the epoxy system. Inferior electrical infiltration threshold of about 0.0031 volume% was reported in case where the measurement was done along the alignment of CNTs.

Wang *et al.* [59] studied the effect of SWCNTs alignment on the properties of epoxy nanocomposites. For the experimental study, SWCNTs were dispersed in the epoxy system using ethanol as the solvent. Alignment of SWCNTs was achieved by drawing the SWCNT/epoxy system in a particular direction and then folding it several times. Three samples were taken into consideration *i.e.* pristine epoxy, epoxy containing SWCNTs aligned parallel to loading and epoxy containing SWCNTs aligned perpendicular to the loading. For the specimen containing SWCNTs aligned parallel to the loading direction, there was an improvement in the elastic modulus and tensile strength with respect increase in SWCNTs content within the epoxy matrix. The tensile strength value increased from 8 MPa to 21.1 MPa at 3 % by weight content of SWCNTs in the epoxy system. It was not the case for specimen containing SWCNTs aligned perpendicular to the loading direction, in which the tensile strength decreased when the content of SWCNTs was increased beyond a certain limit. It was

concluded that with increase in SWCNTs content, problems of agglomeration comes into picture resulting in a decreased mechanical behaviour.

2.2 Functionalization

In case of CNTs, agglomeration or aggregation is a commonly observed problem due to hydrophobic behaviour of CNTs. This leads to reduced mechanical performance of the subsequent nanocomposite. To overcome this shortcoming, functionalization of CNTs is done through the modification of surface of CNTs with the help of some external chemical species. There are ways in which CNTs can be functionalized *i.e.* covalent functionalization and non-covalent functionalization. It has been well established that due to local strains arising in carbon nanotubes owing to pyramidalization and misalignment π-orbitals in the C-atoms, CNTs become more reactive than a regular graphene sheet. This results in attachment of chemical species to CNTs covalently which is known as covalent functionalization of CNTs [60]. Covalent functionalization of CNTs can increase its dispersion in solvents and polymers. Figure 2.2 shows the process of carboxylic functionalization of CNTs.

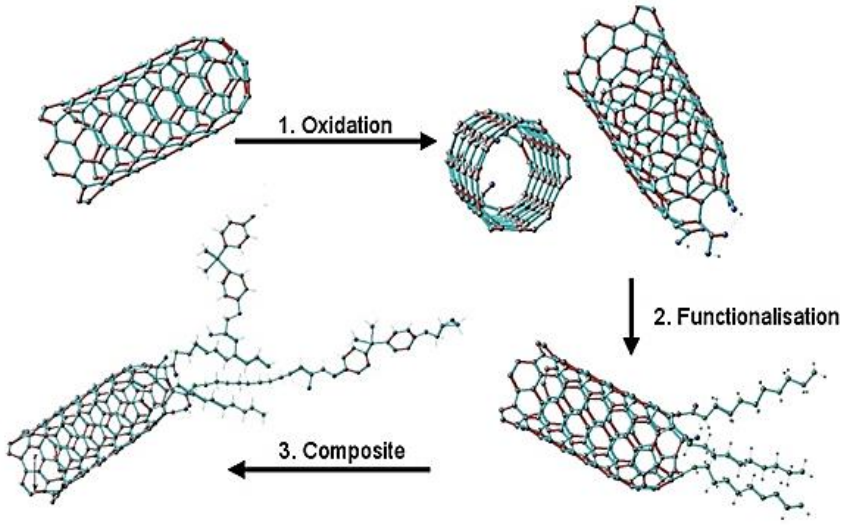

Figure 2.2: Functionalization process [10]

As the first step, an oxidative treatment of the nanotubes is used to develop carboxylic groups. The carboxyl group enables the CNT to create bond with the polymeric resin. In this step, since the CNT cap is opened, the CNT properties are degraded. These carboxyl groups would react with multifunctional amines and form active bonds with these amines in the second step. In the third step, when the resin is added, the active amino functions create bonds with the polymeric molecules of the resin.

In case of non-covalent functionalization of CNTs, van der Waal and π-π interactions play an important role between CNTs and the external chemical species. An advantage of non-

covalent functionalization is that the original structure of CNTs is not affected by the functionalization operation. Chemical functionalization is the most commonly used technique engaged for CNTs in which some external chemical species are attached to CNTs, usually done by solvent assisted techniques. It prevents the individual graphene layer from agglomeration in the course of reduction procedure, whereas sustaining the properties of the former.

Study conducted by Frankland *et al.* [61] exhibited that a good enhancement can be achieved in the mechanical properties of a resin even if only 1% of the carbon atoms interact with the polymer molecules. Additionally, covalent functionalization can offer as a means for engineering the CNT/polymer interface for optimum composite properties. With respect to the mechanical properties of the nanocomposite, improved interfacial adhesion between CNTs and the surrounding polymer molecules either due to covalent and non-covalent functionalization helps in maximizing the load transfer between the polymer matrix and CNTs. With the help of images obtained after SEM characterization, silane functionalized CNTs were observed to be more uniformly dispersed with less amount of agglomeration.

Ma *et al.* [62] examined the effects of covalent functionalization of silane molecules on the properties of MWCNTs reinforced epoxy nanocomposites. Two cases were considered *i.e.* nanocomposite with functionalization and nanocomposite without functionalization. Different samples of nanocomposite containing 0.05 %, 0.10 %, 0.25% and 0.50 % by weight content of MWCNTs were considered for the study. Flexural test and compaction test were employed to validate the mechanical performance of the unmodified and modified epoxy nanocomposite. Moreover, thermal stability of the nanocomposite containing silane functionalized MWCNTs was found to be better to its counterpart. An increase in elastic modulus and flexural strength was witnessed with increase in MWCNTs % by weight content in the epoxy matrix. Fracture toughness of the nanocomposite containing silane functionalized MWCNTs was better in comparison to nanocomposite containing untreated MWCNTs.

Sun *et al.* [63] studied the mechanical properties of CNT reinforced epoxy composites. Oxidized and surface functionalized SWCNTs were used as the reinforcement in the study. Four samples were investigated in the study *i.e.* neat epoxy, p-SWCNTs reinforced epoxy composite, f-SWCNTs reinforced epoxy composite and PAMAM functionalized epoxy. p-SWCNTs means pure SWCNTs were used as the reinforcement with no surface functionalization. f-SWCNTs means that functionalization and oxidation of SWCNTs has been done using polyamidoamine (PAMAM). It was witnessed that due to surface functionalization, there was an improvement in dispersion and adhesion of SWCNTs within the epoxy matrix. Though not significant, there was an augmentation in the mechanical properties of epoxy

matrix. A rise in elastic modulus and tensile strength by 18% and 16% for p-SWCNT reinforced epoxy composite and rise of 27% and 17% for f-SWCNT reinforced epoxy composite was observed.

2.3 Toughening of Nanocomposites

Ever since the discovery of CNTs, researchers have modelled the toughening potentials of CNTs in nanocomposites. Centred on the studies conducted by several researchers over the last two decades, nanocomposites are assumed to demonstrate enhanced fracture toughness upon the introduction of CNTs as the reinforcement Nano filler. The excellent mechanical properties of Nano fillers helps in raising the mechanical performance of the subsequent nanocomposite. Moreover, higher fracture toughness values of nanocomposites leads to their better life which is a common expectation from the composite materials. An important aspect of the studies concerning reinforcement of CNTs is the wide variation in reported enhancement, which arises due to technical difficulties involved in processing of nanocomposites. Based on the literature survey, the main toughening/fracture mechanisms responsible for the enhancement of toughness in CNT reinforced nanocomposites are [8, 9, 11, 64]

1. CNT debonding
2. CNT pull-out
3. Plastic void growth
4. CNT rupture
5. Crack bridging
6. Crack deflection

Schematic representation of possible different types of fracture mechanisms accountable for the toughening of nanocomposites are presented in Figure 2.3. These different fracture mechanism follows when the path of crack growth bump into CNTs present within the polymer matrix. Figure 2.3 (a) presents the original state of CNT in the matrix. Figure 2.3 (b) and (c) illustrates the pull out and rupture phenomenon occurring in CNTs. CNT pull out occurs after the debonding operation. Figure 2.3 (d) presents the telescopic pull out and the fracture of the outermost layer of CNT. Telescopic pull out of outer layer generally happens in case of MWCNTs, which is also referred as the sword in sheath pull out fracture mechanism. In Figure 2.3 (d), partial bridging of the inner layer of CNT is taking place. Lastly, Figure 2.3 (e) presents the bridging operation which often leads to interface failure. Partial debonding of the outer layer of CNT also contributes to interface failure.

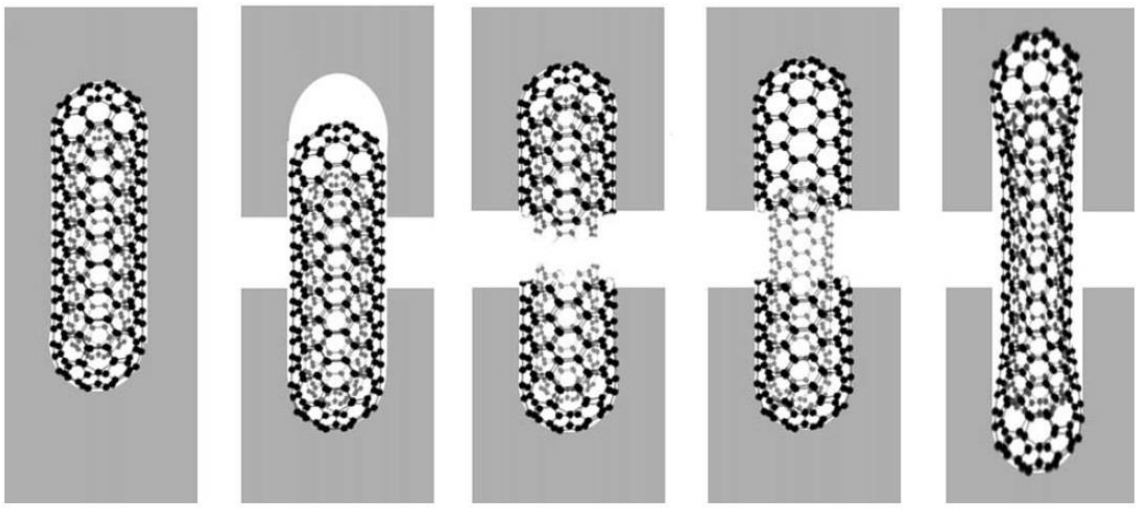

Figure 2.3: Different fracture mechanisms of CNTs [9]

Tai *et al.* [8] used SWCNTs as the reinforcements/fillers to observe the influence of SWCNTs content on the subsequent mechanical properties of phenolic nanocomposites. For the testing purpose, a several specimens were used in which % by weight content of SWCNT varied up to 2%. Results exhibited an improvement in the mechanical properties of the phenolic composites. The elastic modulus increased by over 23.6 %, 28.6 %, 29.6 %, 25.5 %, 25.1 % and 20.1 % corresponding to specimens containing 0.25 %, 0.5 % , 0.75 %, 1.0 %, 1.5 % and 2.0 % by weight content of SWCNTs in the phenolic matrix. Maximum elastic modulus increment was 29.7 % corresponding to specimen containing 0.75 % by weight content of SWCNTs. Similarly, there was an increase in tensile strengths by 11.1 %, 16.6 %, 16.8 %, 16 %, 18.6 %, and 20.3 % corresponding to used specimens. Moreover, during the tensile tests of the specimens, there was no variation in the Poisson's ratio of the specimens. A linear trend in the graph was obtained between stress and strain before the fracture point of the specimens used for study. It was also observed that with high loading of CNTs in the matrix, there was a decrease in the mechanical properties of the resulting composite. For that theoretical study of the elastic modulus of the composite, there was a successful implementation of Halpin-Tsai equations.

Gojny *et al.* [9] studied the influence of three types of CNTs on surface functionalization and mechanical performance of modified epoxy nanocomposite. Single-walled CNTs, double-walled CNTs and multi-walled CNTs were used as the reinforcement filler material in the study with DGEBA based epoxy as the matrix. In order to attain appropriate dispersion CNTs within the epoxy matrix, calandering technique was used. Figure 2.4 and 2.5 illustrates the results of the experimental study.

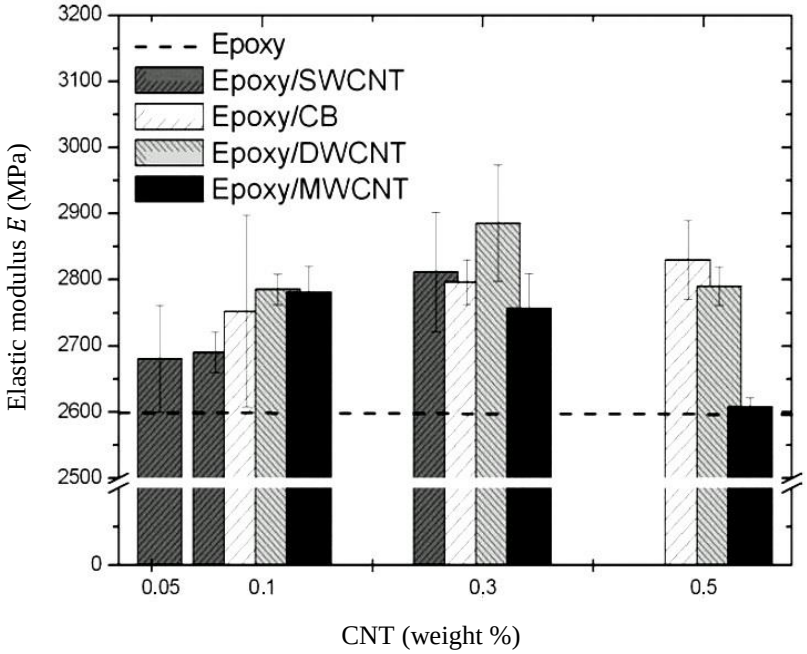

Figure 2.4: Comparison of elastic modulus for different weight content of CNTs [9]

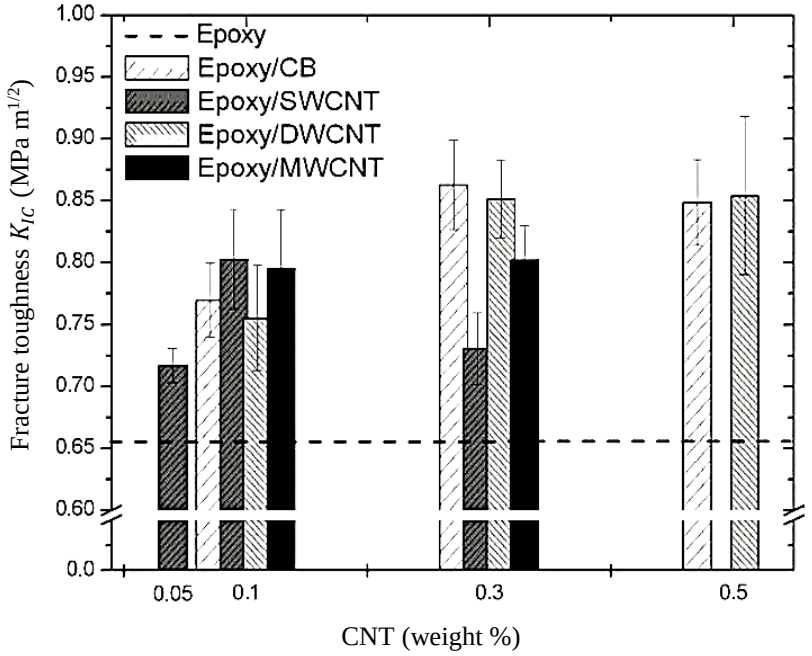

Figure 2.5: Comparison of fracture toughness for different weight content of CNT [9]

In Figure 2.4, results of the elastic modulus has been shown for pure epoxy, epoxy reinforced with Carbon Black (CB), epoxy reinforced with SWCNTs, epoxy reinforced with DWCNTs and epoxy reinforced with MWCNTs. Similarly, Figure 2.5 shows the results for fracture toughness. Results of the work also showed that surface functionalization also plays an important role in the resulting mechanical properties of the nanocomposite. There was a positive influence of amino functionalization on the properties of the nanocomposite *i.e.* fracture

toughness corresponding to 0.3% by weight content of DWCNT-NH_2 reinforced epoxy was 42% higher in comparison to pristine epoxy. In the study, the toughening mechanisms proposed were CNTs pull-out, CNTs rupture, bridging and debonding of the CNTs from the surrounding polymer. There was no modelling work in the study to show the potential of each type of CNTs and to correlate the results to the model. In an additional study conducted by Gojny and Schulte [10] using MWCNTs as the reinforcement in the epoxy matrix, improvement in thermal stability of the subsequent nanocomposite was reported.

Hsieh *et al.* [11] conducted the study using MWCNTs as the reinforcement fillers. The fracture toughness and cyclic performance of the modified epoxy nanocomposite were evaluated by conducting a variety of tests. MWCNTs having length in micrometres and diameter in nanometres were used as the reinforcement. For the matrix base, a DGEBA epoxy matrix system was considered. Tension and fracture toughness tests were conducted for the determination of mechanical properties of the subsequent nanocomposite.

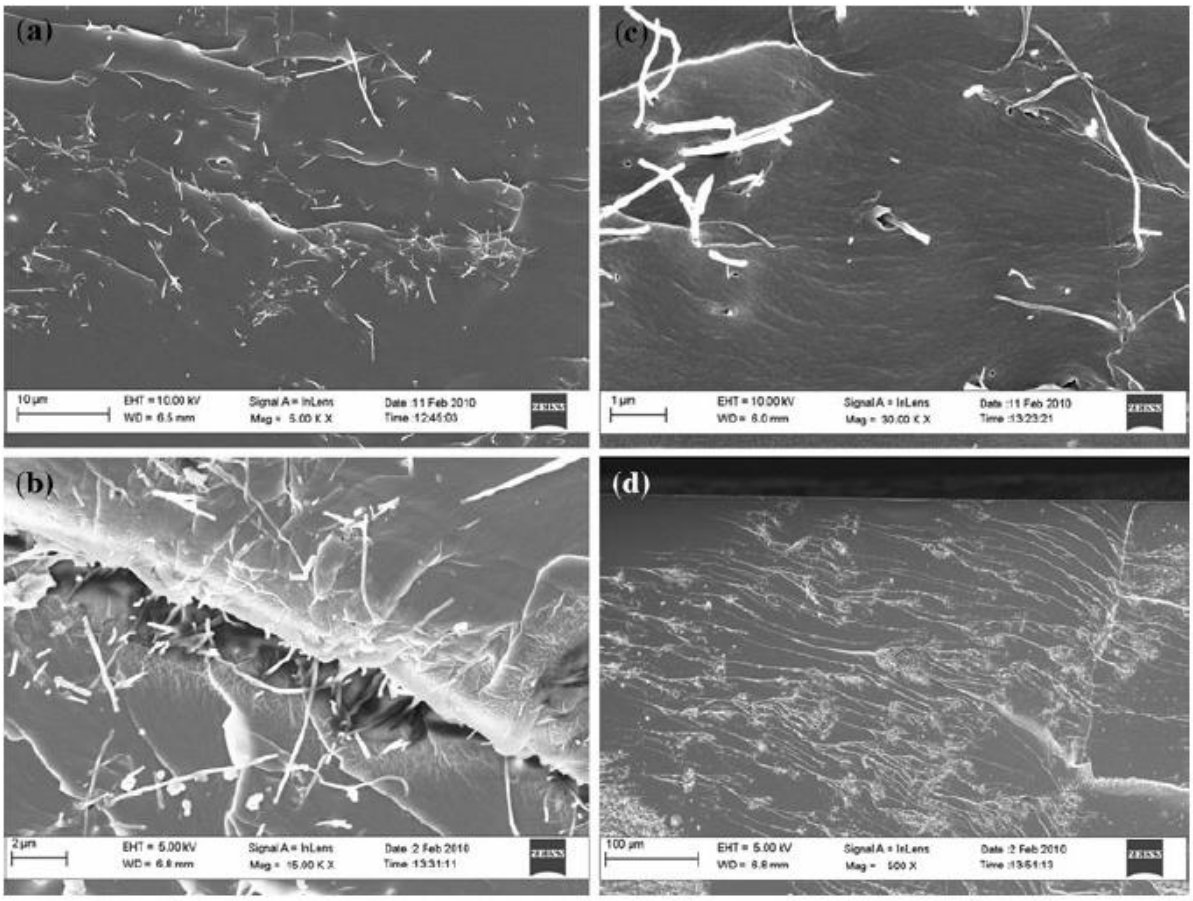

Figure 2.6: FEG-SEM characterization of nanocomposite illustrating (a) Pull-out of CNTs (b) Bridging of CNTs (c) Voids around CNTs and (d) Dispersion of CNTs [11]

Results of the tensile tests revealed that with increase in weight content of MWCNTs in the epoxy matrix, there was an increment in stiffness and mode I fracture toughness of the resulting

nanocomposite. For the epoxy reinforced with 0.5 % by weight content of MWCNTs, there was an increment of 12% in the elastic modulus compared to that of pure epoxy. Additionally, fracture toughness K_{IC}, and fracture energy G_C values of the epoxy polymers amplified progressively as the % by weight content of MWCNTs was increased inside the epoxy matrix. The results showed that there was 67 % increase in the fracture energy compared to that of unmodified epoxy at 0.5 % by weight content of MWCNTs in the epoxy system. CNT pull-out followed by debonding and plastic void growth were considered as the major toughening mechanisms contributing to the rise in fracture energy of the subsequent nanocomposite. The three different fracture mechanisms were visible by examination conducted using FEG-SEM. CNT pull out and bridging was observed in the Figure 2.6 (a) and 2.6 (b). Figure 2.6 (c) indicates the voids caused by debonding of CNTs in the matrix followed by plastic void growth.

An additional research was conducted by Hsieh *et al.* [65] to study the improvement in mechanical properties of the nanocomposite by reinforcing both silica nanoparticles and MWCNTs in an epoxy matrix. AFM and TOM were used to inspect the subsequent nanocomposite. The results revealed a consistent dispersion of nano-silica inside the epoxy matrix with a slight agglomeration of MWCNTs. The unmodified epoxy matrix recorded a value of 2.9 GPa as the elastic modulus. The reinforcement of 0.06 % weight content of MWCNTs and 2.0 % by weight content of nanosilica augmented the stiffness by around 1.7%. By reinforcing 6.0 % by weight content of nano-silica, the recorded value for elastic modulus was 3.0 GPa. Whereas, the addition of 0.06 % by weight content of MWCNTs to 6.0 % by weight content of nano-silica amplified the elastic modulus soberly by only 0.6%.

Tang *et al.* [13] studied the fracture mechanisms in epoxy filled reinforced with ozone functionalized MWCNTs. Ozone-treated MWCNTs were used as the potential reinforcement fillers in the epoxy matrix. An improvement in fracture toughness and strength of the modified epoxy was observed in comparison to pristine epoxy. Moreover ozone functionalization helped in better dispersion and strong interfacial bonding of MWCNTs with the epoxy matrix.

Ladani *et al.* [14] conducted the study on epoxy nanocomposites using aligned nanofibres as the reinforcements. The fracture energies of modified nanocomposites were calculated by taking double cantilever beam specimens into consideration for the mechanical testing purpose. The experimentation specimens consisted different concentration of carbon nanofibres (up to 1.6 wt. %). The results showed the increase in electrical conductivity of the epoxy nanocomposite by seven orders of magnitude up to 10^{-2} S/m when 1.6 wt. % carbon nanofibres were used as the reinforcements. Similarly, based on results of fracture toughness

tests, fracture energy of the epoxy nanocomposite increased by 1600 % *i.e.* from 134 to 2345 J/m^2.

Ayatollahi *et al.* [66] examined the influence of % by weight content of MWCNTs on the mechanical performance of modified epoxy nanocomposites, under bending and shear loading conditions. Three dissimilar reinforcements *i.e.* 0.1 %, 0.5 % and 1 % by weight content of MWCNTs were used in the study. For the fracture testing, a three point bend specimen and a four point bend specimen (ASFPB) were used to estimate the mode I and mode II fracture toughness values. The results for all the specimens exhibited a linear elastic and brittle behaviour of the tested specimens. The results revealed an improvement in the mode I and mode II fracture toughness of the modified epoxy nanocomposite, when the % by weight content of MWCNTs was increased from 0.1 % to 0.5 % within the epoxy system. The results also showed a much improved fracture toughness of nanocomposite under shear loading as compared to the normal loading. From this result, dependence of the fracture toughness on the typing of loading was concluded. The rise in mode I and mode II fracture toughness can be more clearly observed from Figure 2.7.

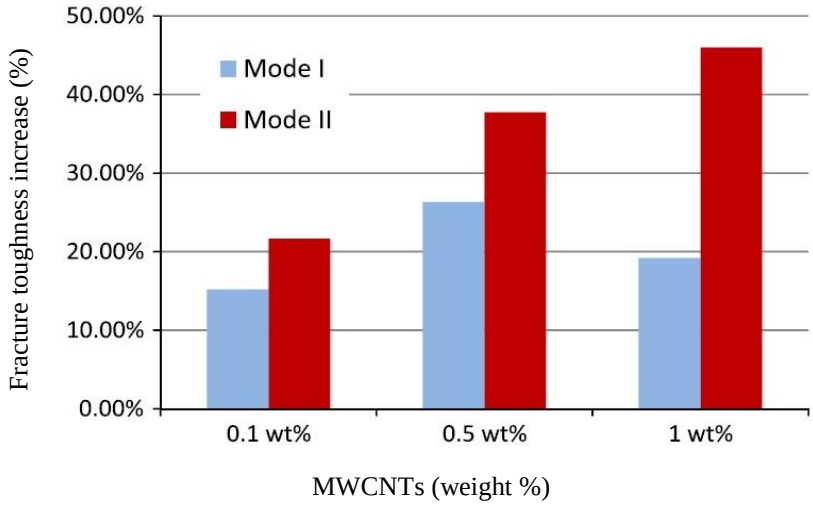

Figure 2.7: Increase in fracture toughness for different weight content of MWCNTs [66]

In another study conducted by Ayatollahi *et al.* [67] on the mixed mode fracture in MWCNT reinforced epoxy nanocomposite, it was concluded that the improvement in fracture resistance of the modified nanocomposite depends on the mode mixity. For the fracture toughness testing, experimental specimens were produced taking both unmodified epoxy and modified epoxy with three different % weight content of MWCNTs in the epoxy system *i.e.* 0.1 %, 0.5 % and 1 %. It was concluded that some additional mechanisms were contributing in mixed mode and mode II fracture of nanocomposites which were not taken into consideration in the conservative fracture criterions.

Yang *et al.* [68] investigated the cryogenic mechanical behaviour in CNT reinforced nanocomposites. In the study, DGBEF/DETD epoxy system modified by polyethersulfone was reinforced using MWCNTs. The results revealed that the tensile strength and elastic modulus improved by 57.9% and 10.1%, respectively at 77 K temperature. The fracture toughness increased by about 13.5 % at 0.5 % by weight content of MWCNTs content with a value of 2.02 MPa $m^{1/2}$ compared to a value of 1.78 MPa $m^{1/2}$ of PES modified epoxy matrix.

Chen *et. al.* [69] in their study, reinforced epoxy matrix with MWCNTs to improve the cryogenic behaviour of resulting nanocomposite. Ultrasonic mixing technique was employed for the dispersion of MWCNTs in the epoxy matrix. In order to achieve optimum interfacial bonding between the MWCNTs and the epoxy polymer, temperature was lowered down to liquid nitrogen temperature. Due to large differences between the thermal expansion coefficients of MWCNTs and the epoxy polymer, strong interfacial bonding was witnessed. Further on the basis of the experimental test results for both the cases of nanocomposite preparation *i.e.* at room temperature and cryogenic temperature of 77 K, higher values of elastic modulus and tensile strength was observed for the nanocomposite prepared at 77 K. Impact strength of the epoxy matrix was also improved at both room temperature and 77 K. For the 0.5 % by weight content of MWCNTs in the epoxy, impact strength got improved by around 76.7 and 51.4%.

2.4 Conclusions from Literature Review

On the basis of literature review of CNT reinforced polymer nanocomposites, following conclusions can be drawn

i. The mechanical performance of the Nanocomposites can be enhanced significantly at a relative low CNT content within the matrix.
ii. Better dispersion of CNTs in the polymer matrix leads to improved mechanical properties of the CNT reinforced nanocomposites. The CNTs alignment also have a role to play in the subsequent mechanical properties of the nanocomposite.
iii. Surface functionalization plays a vital role in achieving strong interfacial bonding between the CNTs and the surrounding polymer matrix. It also helps in improving the dispersion of CNTs leading to higher toughness values of the subsequent nanocomposites. Appropriate functionalization process can be used *i.e.* physical or chemical functionalization depending upon the interactions between CNT and the surrounding polymer molecules.

iv. A significant improvement in the properties of nanocomposite can be obtained by attaining good interfacial bonds between the matrix and the reinforcement phase often leading better load transfer.

v. The major fracture energy toughening criterions in CNT reinforced nanocomposites are CNT pull out, sword in sheath mechanism in case of MWCNTs, CNT debonding, CNT rupture and plastic void growth after debonding.

vi. In case of CNTs having aspect ratio on the higher side, there is a parameter termed as critical length of CNT bridging which will be responsible for other toughening mechanisms.

2.5 Objective

The objectives of the present work are as follows

i. To evaluate the equivalent properties of the nanocomposite using both SWCNTs and MWCNTs as the reinforcement in the polymer matrix. The equivalent properties comprises elastic modulus, Poisson's ratio, fracture energy and fracture toughness of the subsequent nanocomposite. In the present work, epoxy has been considered as the matrix phase and different fracture mechanisms of CNT contributes to the improvement in toughness value of the epoxy.

ii. To simulate crack growth using XFEM in a rectangular thin plate containing an edge crack. The equivalent properties corresponding to both SWCNT reinforced nanocomposite and MWCNT reinforced nanocomposite will be used as the material parameters of the thin rectangular plate.

iii. To simulate crack growth using XFEM in a rectangular thin plate containing a centre crack. The equivalent properties corresponding to both SWCNT reinforced nanocomposite and MWCNT reinforced nanocomposite will be used as the material parameters of the thin rectangular plate.

Chapter 3

Mathematical Modelling

This chapter contains the mathematical modelling required to estimate the equivalent properties of the CNT reinforced nanocomposite. Estimation of equivalent properties in CNT reinforced polymer nanocomposite is a critical part of this work, as it provides the material parameters required as the input for crack growth simulation study conducted using XFEM approach. The equivalent properties of the nanocomposite have been evaluated on the basis of known properties of the matrix and CNTs. For the computation of equivalent properties, CNTs are considered to be in random orientation within the matrix to account different types of dispersion processes such as ultrasonification, mechanical mixing, sonification, etc. In the present study, elastic modulus, Poisson's ratio, fracture energy and the fracture toughness of the CNT reinforced nanocomposite have been evaluated using micromechanical models.

3.1 Elastic Modulus

Evaluation of the elastic modulus of the CNT reinforced polymer nanocomposite is the first step of this study. In the present work, the elastic modulus of the nanocomposite has been computed using Halpin-Tsai modelling approach which deals with the micromechanics of reinforcement and the matrix. Halpin-Tsai approach is a widely adopted mathematical modelling approach used for predicting the elastic properties of unidirectional, short fibre-reinforced composites. Halpin-Tsai approach considers the elastic properties of a composite material as the function of CNT content, aspect ratio and elastic modulus of its individual components [70, 71]. Figure 3.1 presents the layout for computation of elastic properties of the CNT reinforced polymer nanocomposite using Halpin-Tsai approach.

The Halpin-Tsai equations correlates the property of nanocomposite with the characteristics of the matrix and reinforcement phase accompanied by their proportions and geometries. According to Halpin-Tsai approach, the elastic modulus in the longitudinal (E_{11}) and transverse direction (E_{22} or E_{33}) is expressed in a general form as provided in equation (3.1).

$$E = \left(\frac{1 + \xi\eta V_{NT}}{1 - \eta V_{NT}}\right) E_m \tag{3.1}$$

where E and E_m represents the elastic modulus of nanocomposite and the matrix; V_{NT} represents the volume fraction of the CNT and η is given by equation (3.2).

$$\eta = \frac{\left(\frac{E_{NT}}{E_m}\right) - 1}{\left(\frac{E_{NT}}{E_m}\right) + \xi} \tag{3.2}$$

where E_{NT} represents the elastic modulus of CNT; ξ represents the shape factor which depends on the geometry and loading direction of CNT.

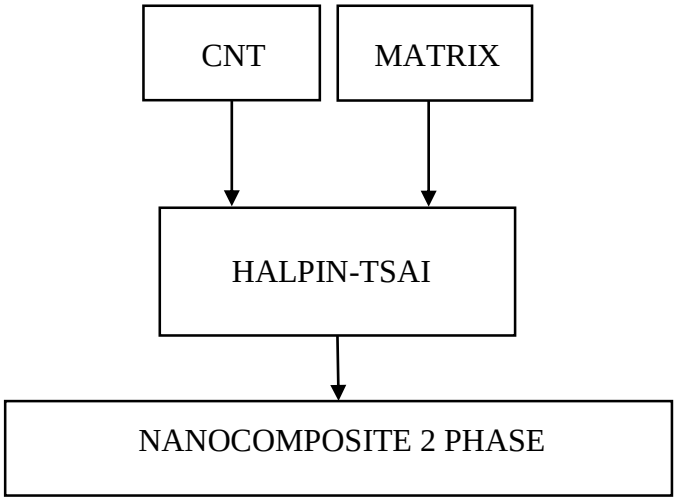

Figure 3.1: Layout for computing the elastic properties of CNT reinforced nanocomposites

The shape factor is given by equation (3.3).

$$\xi = 2(l_{NT} / d_{NT}) \tag{3.3}$$

The shape factor expression provided in equation (3.3) corresponds to the longitudinal elastic modulus E_{11}, where l_{NT} and d_{NT} represents the length and diameter of the reinforcement (CNT) respectively [70]. When ξ = 2, on the other hand, the same equation can be used for calculating the transverse modulus E_{22} or E_{33}. The elastic modulus of randomly oriented CNT reinforced nanocomposite based on modified Halpin-Tsai equations can be expressed as equation (3.4).

$$E_{NC} = \left[\frac{3}{8}\left(\frac{1 + \xi\eta_L V_{NT}}{1 - \eta_L V_{NT}}\right) + \frac{5}{8}\left(\frac{1 + 2\eta_D V_{NT}}{1 - \eta_D V_{NT}}\right)\right] E_m \tag{3.4}$$

where,

$$\eta_L = \frac{\left(\frac{E_{NT}}{E_m}\right) - 1}{\left(\frac{E_{NT}}{E_m}\right) + \xi} \tag{3.5}$$

$$\eta_D = \frac{\left(\frac{E_{NT}}{E_m}\right) - 1}{\left(\frac{E_{NT}}{E_m}\right) + 2} \tag{3.6}$$

Thostenson and Chou [72] amended the Halpin-Tsai theory for MWCNTs. It was suggested that in case of MWCNTs, simply the outer layer of MWCNTs is carrying the entire load transferred at the CNT/matrix interface. This is due to the reason that the bonding between the walls in MWCNTs takes place due to van der Waals interactions, which are relatively weak in nature. As a result, minimum load transfer will take place between the layers of CNTs. According to this, the effective CNT modulus can be represented in terms of elastic modulus, layer thickness (t_{NT}) and diameter of CNT as shown in equation (3.7).

$$E_{eff} = \frac{4t_{NT}}{d_{NT}} E_{NT} \tag{3.7}$$

The above expression is valid only when $(t_{NT}/d_{NT}) < 0.25$. Using the equation (3.7), equation (3.5) and (3.6) can be modified into equation (3.8) and (3.9).

$$\eta_L = \frac{\left(\frac{E_{NT}}{E_m}\right) - \left(\frac{d_{NT}}{4t_{NT}}\right)}{\left(\frac{E_{NT}}{E_m}\right) + \left(\frac{l_{NT}}{2t_{NT}}\right)} \tag{3.8}$$

$$\eta_D = \frac{\left(\frac{E_{NT}}{E_m}\right) - \left(\frac{d_{NT}}{4t_{NT}}\right)}{\left(\frac{E_{NT}}{E_m}\right) + \left(\frac{d_{NT}}{2t_{NT}}\right)} \tag{3.9}$$

3.2 Volume Fraction & Poisson's Ratio

For the conversion of measured weight fraction of CNTs to its equivalent volume fraction, density of the CNTs and polymer matrix must be known. Using the principle pertaining to rules of mixture, CNTs volume fraction in the matrix can be evaluated based on the density of the constituents using equation (3.10).

$$V_{NT} = \frac{\rho_c}{\rho_{NT}} m_{NT} \tag{3.10}$$

where,

$$\rho_c = \rho_{NT} V_{NT} + \rho_m V_m \tag{3.11}$$

In equation (3.11), ρ represents the density; and subscripts *NT*, *m* and *c* refers to CNT, matrix and nanocomposite.

Further, on substituting equation (3.11) in (3.10), the volume fraction can be calculated using equation (3.12).

$$V_{NT} = \frac{m_{NT}}{m_{NT} + (\rho_{NT}/\rho_m) - (\rho_{NT}/\rho_m) m_{NT}} \tag{3.12}$$

Similarly, the Poisson's ratio of the resulting nanocomposite can be obtained based on the rules of mixture as per equation (3.13).

$$\nu_c = \nu_{NT} V_{NT} + \nu V_m \tag{3.13}$$

where ν_{NT} represents the Poisson's ratio of CNT; ν represents the Poisson's ratio of matrix; and ν_c represents the Poisson's ratio of nanocomposite.

3.3 Fracture Energy

For estimating the fracture energy of the CNT reinforced polymer nanocomposite, CNT pull out and CNT debonding have been considered as the main fracture energy toughening criterions [11]. Apart from pull out and debonding, plastic void growth is also a common toughening mechanism liable for the rise in fracture energy. But in this study, platic void growth after debonding in the matrix has not been considered as the toughening mechanism, due to its lower contribution in increase of fracture energy which can be neglected. First major toughening mechanism is CNT pull out which occurs after the debonding process. Blanco *et al.* [73] studied the mode I fracture in composites reinforced using aligned CNTs. CNT pull out or sword in sheath pull out was considered as the responsible toughening mechanism, contributing to increase in fracture energy. Sword in sheath pull out is related to fracture mechanism occurring in MWCNTs. In this process, the outer shell of CNT gets fractured in tension and the inner shells are pulled out from inside. The broken outer shell remain embedded in the polymer due to this fracture process.

According to Hsieh *et al.* [11] and the analysis done by Hull and Clyne [46] for fibres, fracture energy $\Delta G_{pull-out}$ required to pull out a CNT can be given by equation (3.14). The relation shows the product of the number of CNTs involved and the energy required to pull out each CNT.

$$\Delta G_{pull-out} = \int_0^{l_{po}} \frac{N dx}{l_{po}} \pi r_{NT} x^2 \, \tau_i \tag{3.14}$$

where x represents the length involving in pull out mechanism; l_{po} represents the pull out length of CNT from matrix; r_{NT} represents the radius of CNT; and τ_i represents the interfacial shear strength between matrix and CNT. Blanco *et al.* [73] provided the values ranging between 1 and 100 MPa for the interfacial strength. Barber *et al.* [74] suggested an average interfacial shear strength value of 47 MPa for CNT-polyethylene interface system.

The total number of CNTs per unit area N is given by equation (3.15).

$$N = \frac{V_{fpo}}{\pi {r_{NT}}^2} \tag{3.15}$$

where, V_{fpo} represents the volume fraction of the CNTs getting pulled out from the matrix.

Substituting the equation (3.15) into (3.14), and then integrating, equation (3.16) is obtained.

$$\Delta G_{pull-out} = \frac{V_{fpo} {l_{po}}^2 \tau_i}{3 r_{NT}} \tag{3.16}$$

The total fracture energy associated with CNTs pull-out is divided into two cases. In the first case, length of the CNT is smaller than the critical length of CNT. In this situation, all the CNTs undergoes pull-out process. In the second case, length of the CNT is larger than the critical length of CNT. In this scenario, a portion of CNTs undergoes pull-out process and the rest exhibit rupture. The number of CNTs participating in pull-out process are proportional to (l_c/l_{NT}) and the number of CNTs participating in the rupture are proportional to $(1 - l_c/l_{NT})$. More explicitly, $V_{fpo}(l_c/l_{NT})$ fraction of CNTs participate in the pull-out process and $V_{fpo}(1 - l_c/l_{NT})$ fraction of CNTs participate in the rupture process. It is to be taken into notice that the CNT pull out length will not be equal to the total length of the CNT, as only a certain percentage of the CNT is getting pulled out from the matrix. Thus, the longest possible pull-out length of the CNT is taken as half the length of CNT *i.e.* $(l_{NT}/2)$, when the CNT is smaller than the critical length of CNT. Similarly, the longest possible pull-out length of the CNT is taken as half the critical length *i.e.* $(l_c/2)$, when the length of CNT is larger than the critical length of CNT. The critical length of the CNTs is given by equation (3.17) based on the analysis done by Kelly and Tyson [75].

$$l_c = \frac{\sigma_{NT} d_{NT}}{2\tau_i} \tag{3.17}$$

where, σ_{NT} represents the strength of CNTs; and l_c represents the critical length of CNT. The fracture energy [76] associated with elastic deformation of CNTs prior to rupturing can be expressed using equation (3.18).

$$\Delta G_{rupture} = \frac{V_{fpo}\, \sigma_{NT} l_{NT} \epsilon_{max}}{2}\left(1 - \frac{l_c}{l_{NT}}\right) = \frac{V_{fpo}\, {\sigma_{NT}}^2 l_{NT}}{2E_{NT}}\left(1 - \frac{l_c}{l_{NT}}\right) \tag{3.18}$$

where, E_{NT} and ϵ_{max} are the elastic modulus and tensile failure strain of CNT.

The second major toughening mechanism is the interfacial debonding which occurs prior to CNT pull-out. It is an essential process as it minimises the constraint near crack tip by allowing the CNTs to get pulled out from the matrix, and thereafter the matrix deforms plastically with the help of void growth. The CNT and polymer interfacial debonding energy ΔG_{db} [11], is given by equation (3.19).

$$\Delta G_{db} = \frac{V_{fdb} l_{NT} G_i}{d_{NT}} \tag{3.19}$$

where, V_{fdb} is the volume fraction of the CNTs which are getting debonded from the matrix; and G_i is the interfacial fracture energy between the CNTs and the matrix.

Barber *et al.* [74] suggested the values ranging between 13 and 34 J/m^2 for interfacial fracture energy (G_i). In the present work, a value of 25 J/m^2 will be used for the interfacial fracture energy. Moreover, the values of volume fraction of the CNTs (getting debonded and pulled out) have been assumed to be equal to that of volume fraction of CNTs calculated theoretically. Though practically during experiments, all the CNTs might not participate in the toughening process. The final relation for the fracture energy of CNT reinforced nanocomposite can be expressed using equation (3.20).

$$G_C = G_{CU} + \Delta G_{pull-out} + \Delta G_{db} + \Delta G_{rupture} \tag{3.20}$$

where, G_{CU} represents the fracture energy of unmodified polymer matrix. A fracture energy value of 133 J/m^2 has been considered for the unmodified epoxy in the present work.

3.4 Fracture Toughness

Fracture toughness of CNT reinforced polymer nanocomposite is the most important parameter in the crack growth simulation study. From the definition point of view, it is parameter describing the ability of the material containing the crack, to resist fracture. The value for fracture toughness of a material can be accurately estimated by critical stress intensity factor (K_{IC}) or critical strain energy release rate (G_C) values [53]. Stress Intensity Factor (SIF) is a local parameter that helps in quantifying the magnitude of stress, strains and displacements fields near the tip of a discontinuity. More specifically, it helps in quantifying the magnitude of stress singularity near the crack tip. Similarly, strain energy release rate (G) is defined as the decrement in total potential energy per unit crack extension. It can also be called as the force responsible for the crack extension and the critical value of strain energy release rate is the fracture energy associated with crack extension. For the present work, fracture toughness of the CNT reinforced polymer nanocomposite can be obtained in terms of these two parameters. But for the theoretical calculations, stress intensity factor values are more tractable in comparison to strain energy release rate values. In the present work, fracture toughness for the crack growth simulation has been used in terms of critical stress intensity factor values. In fracture mechanics, the critical stress intensity factor value can be related to critical energy release rate [53] using the relation given in the equation (3.21).

$$G_C = {K_{IC}}^2 \left(\frac{1-\nu^2}{E}\right) \tag{3.21}$$

where E represents the elastic modulus; and ν represents the Poisson's ratio of the material. The equation (3.21) is derived using the assumption that the material is isotropic, homogeneous, and linearly elastic. In the relation provided in equation (3.21), plane strain conditions have been assumed and the crack extends along the direction of the initial crack. Similarly, for plane stress conditions, the equivalent relation [53] can be given by equation (3.22).

$$G_C = {K_{IC}}^2 \left(\frac{1}{E}\right) \tag{3.22}$$

3.5 XFEM Formulation

Extended finite element method (XFEM) is an effective numerical technique to simulate crack evolution in materials subjected to external loadings. The concept of partition of unity forms the fundamental mathematical basis behind XFEM. In XFEM, a discontinuity is modelled independent to the mesh using a set of local enrichment functions derived from the theoretical background of the crack growth problem. The application of these enrichment functions is to model the displacement field close to crack face/split (discontinuous field) and the crack tip (asymptotic field).

3.5.1 Governing Equations

For the development of governing equations, a domain Ω has been taken into consideration. The boundary of the domain is sub-divided into displacement Γ_u, traction Γ_t and traction-free Γ_c boundaries as illustrated in Figure 3.2. The strong form of the equilibrium condition [77] is given by equation (3.23).

$$\nabla . \boldsymbol{\sigma} + \boldsymbol{F_b} = 0 \text{ in } \Omega \tag{3.23}$$

where ∇ represents the gradient operator; $\boldsymbol{F_b}$ represents the body force per unit volume; and $\boldsymbol{\sigma}$ represents the Cauchy stress-tensor.

It has been taken into assumption that the material will show linear elastic behaviour before fracture, and constitutive relation is given by equation (3.24).

$$\boldsymbol{\sigma} = \boldsymbol{D\varepsilon} \tag{3.24}$$

where $\boldsymbol{D}$ represents the elasticity tensor of the material.

Elasticity tensor for a two dimensional isotropic material reduces to equation (3.25) for plane stress scenario and to equation (3.26) for plain strain scenario.

$$\boldsymbol{D} = \frac{E}{1-\nu^2}\begin{bmatrix} 1 & \nu & 0 \\ \nu & 1 & 0 \\ 0 & 0 & (1-\nu)/2 \end{bmatrix} \tag{3.25}$$

$$\boldsymbol{D} = \frac{E(1-\nu)}{(1+\nu)(1+2\nu)}\begin{bmatrix} 1 & \nu/(1-\nu) & 0 \\ \nu/(1-\nu) & 1 & 0 \\ 0 & 0 & (1-2\nu)/[2(1-\nu)] \end{bmatrix} \tag{3.26}$$

where E represents the elastic modulus; and ν represents the Poisson's ratio.

The essential (Dirichlet) and natural (Neumann) boundary conditions are given by equations (3.27) to (3.29).

$$\boldsymbol{u} = \bar{\boldsymbol{u}} \text{ on } \Gamma_u \tag{3.27}$$

$$\boldsymbol{\sigma} . \boldsymbol{n} = \bar{\boldsymbol{t}} \text{ on } \Gamma_t \tag{3.28}$$

$$\boldsymbol{\sigma} . \boldsymbol{n} = 0 \text{ on } \Gamma_c \tag{3.29}$$

where, $\boldsymbol{n}$ represents the unit normal vector acting outwards from the domain; $\bar{\boldsymbol{u}}$ represents the displacement on the boundary Γ_u; and $\bar{\boldsymbol{t}}$ represents the traction acting on the boundary Γ_t.

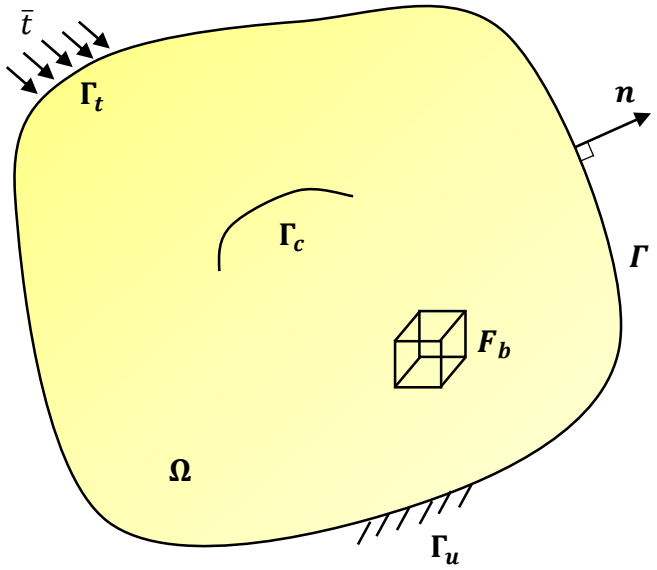

Figure 3.2: Geometry of a domain containing a discontinuity $\boldsymbol{\Gamma_c}$

The equilibrium equation in weak form [18, 20] is expressed by the equation (3.30).

$$\int_{\Omega} \boldsymbol{\sigma} . \delta\boldsymbol{\varepsilon} \, d\Omega = \int_{\Omega} \boldsymbol{F_b} . \delta\boldsymbol{u} \, d\Omega + \int_{\Gamma_t} \bar{\boldsymbol{t}} . \delta\boldsymbol{u} \, d\Gamma \tag{3.30}$$

Thereafter, substitution of trial and test functions in equation (3.30) yields a discrete system of linear equilibrium equations, given by equation (3.31).

$$[\boldsymbol{K}]\{\boldsymbol{u^h}\} = \{\boldsymbol{f}\} \tag{3.31}$$

where $\boldsymbol{K}$ represents the global stiffness matrix; $\boldsymbol{u^h}$ represents the unknown displacements vector; and $\boldsymbol{f}$ represents the external force vector. The global matrix and vectors are calculated by assembling the matrix and vectors of each element.

3.5.2 XFEM Approximation for Crack

In two-dimensional modelling of crack face and crack tips [20, 23] in XFEM, the unknown displacement vector, $\boldsymbol{u^h}$ is written in terms of the standard displacement vector $\boldsymbol{u}$, crack face displacement vector $\boldsymbol{u^H}$ and crack tip displacement $\boldsymbol{u^{tip}}$ vector as given by equation (3.32).

$$\boldsymbol{u^h}(x) = \boldsymbol{u}(x) + \boldsymbol{u^H}(x) + \boldsymbol{u^{tip}}(x) \tag{3.32}$$

or in a more explicit manner,

$$\boldsymbol{u^h}(x) = \sum_{i=1}^{n} N_i(x) \left[\boldsymbol{u_i} + \underbrace{\big(H(x) - H(x_i)\big)\boldsymbol{a_i}}_{i \epsilon n_h} + \underbrace{\sum_{l=1}^{4} (T_l(x) - T_l(x_i))\boldsymbol{t_i}^l}_{i \epsilon n_t} \right] \tag{3.33}$$

where, n represents the total number of nodes obtained after discretization operation, $\boldsymbol{u_i}$ represents the standard displacements vector, $N_i(x)$ represents the shape functions associated with every single node; n_h represents the number of nodes associated with crack split/face elements, $\boldsymbol{a_i}$ represents the displacement vector associated to crack split domain, and $H(x)$ represents the Heaviside function for modelling crack face; n_t represents the number of nodes associated with crack tip domain, $\boldsymbol{t_i}^l$ represents the displacement vector associated with crack tip elements, and $T_l(x)$ represents the crack tip enrichment functions. Figure 3.3 presents a proper schematic representation of split, tip and blending elements along with the nodes associated to them.

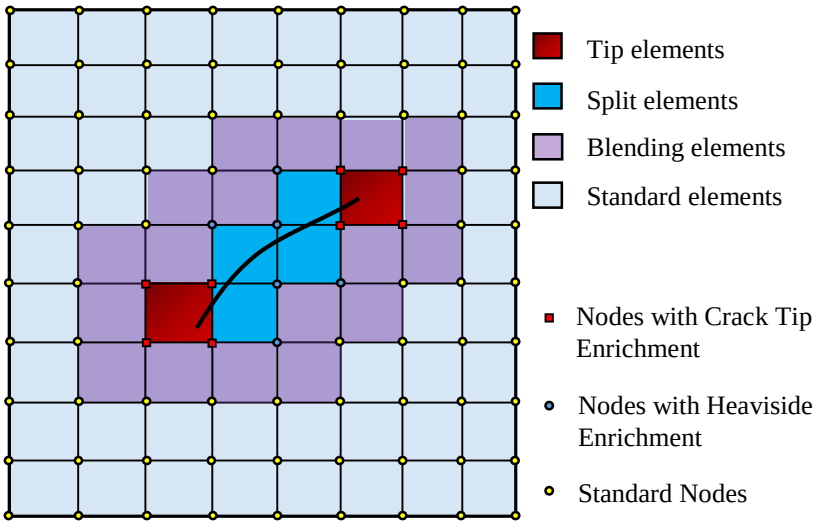

Figure 3.3: Schematic of split, tip, blending and standard elements

Heaviside function (H) is defined as a local enrichment function used for modelling the jump in displacement across the crack face [20]. The discontinuous Heaviside function is expressed using equation (3.34).

$$H(x) = \begin{cases} +1 \; \forall \; \Psi(x) \geq 0 \\ -1 \; \forall \; \Psi(x) < 0 \end{cases} \tag{3.34}$$

where $\Psi(x)$ is termed as the signed distance function which calculates the least distance from the point x to the point x^* on the discontinuity. Its value can be either positive or negative and is generally estimated using the expression given in equation (3.35).

$$\Psi(x) = min\|x - x^*\| sign\left((x - x^*).n_{\Gamma_c}\right) \tag{3.35}$$

where n_{Γ_c} represents the unit normal vector on the contact interface; and x^* represents a point lying on the path of discontinuity.

The asymptotic tip enrichment functions T_l are derived from the analytical solution of stress and displacement fields near the crack tip area [53]. It is usually expressed in terms of the local crack tip polar coordinate system (r, θ) which is given by using equation (3.36).

$$T_l(r, \theta) = \left\{\sqrt{r}\sin\frac{\theta}{2}, \sqrt{r}\cos\frac{\theta}{2}, \sqrt{r}\sin\theta\sin\frac{\theta}{2}, \sqrt{r}\sin\theta\cos\frac{\theta}{2}\right\} \tag{3.36}$$

3.5.3 XFEM Formulation

By taking the approximation function expressed in equation (3.33), the elemental matrices, K and f are obtained by equations (3.37) to (3.46).

$$\boldsymbol{K_{ij}^{e}} = \begin{bmatrix} \boldsymbol{K_{ij}^{uu}} & \boldsymbol{K_{ij}^{ua}} & \boldsymbol{K_{ij}^{ut}} \\ \boldsymbol{K_{ij}^{au}} & \boldsymbol{K_{ij}^{aa}} & \boldsymbol{K_{ij}^{at}} \\ \boldsymbol{K_{ij}^{tu}} & \boldsymbol{K_{ij}^{ta}} & \boldsymbol{K_{ij}^{tt}} \end{bmatrix} \tag{3.37}$$

$$\boldsymbol{f^{h}} = \left\{\boldsymbol{f_i^{u}} \; \boldsymbol{f_i^{a}} \; \boldsymbol{f_i^{t1}} \; \boldsymbol{f_i^{t2}} \; \boldsymbol{f_i^{t3}} \; \boldsymbol{f_i^{t4}}\right\}^T \tag{3.38}$$

The sub-matrices and vectors are given as

$$\boldsymbol{K_{ij}^{rs}} = \int_{\Omega^e} (B_i^r)^T \boldsymbol{D} B_j^s h d\Omega \tag{3.39}$$

where $r, s = u, a, t$.

$$\boldsymbol{f_i^{u}} = \int_{\Omega^e} N_i \boldsymbol{b} d\Omega + \int_{\Gamma_t} N_i \bar{\boldsymbol{t}} \, d\Gamma \tag{3.40}$$

$$\boldsymbol{f_i^{a}} = \int_{\Omega^e} N_i\big(H(x) - H(x_i)\big)\boldsymbol{b} d\Omega + \int_{\Gamma_t} N_i\big(H(x) - H(x_i)\big)\bar{\boldsymbol{t}} d\Gamma \tag{3.41}$$

$$\boldsymbol{f_i^{tl}} = \int_{\Omega^e} N_i\big(T_l(x) - T_l(x_i)\big)\boldsymbol{b} d\Omega + \int_{\Gamma_t} N_i\big(T_l(x) - T_l(x_i)\big)\bar{\boldsymbol{t}} d\Gamma \tag{3.42}$$

where $l = 1, 2, 3 \; and \; 4$.

$$B_i^r = \begin{bmatrix} N_{i,x} & 0 \\ 0 & N_{i,y} \\ N_{i,y} & N_{i,x} \end{bmatrix} \tag{3.43}$$

$$B_i^a = \begin{bmatrix} \left(N_i\left(H(x) - H(x_i)\right)\right)_{,x} & 0 \\ 0 & \left(N_i\left(H(x) - H(x_i)\right)\right)_{,y} \\ \left(N_i\left(H(x) - H(x_i)\right)\right)_{,y} & \left(N_i\left(H(x) - H(x_i)\right)\right)_{,x} \end{bmatrix} \tag{3.44}$$

$$B_i^t = [B_i^{t1}\ B_i^{t2}\ B_i^{t3}\ B_i^{t4}] \tag{3.45}$$

$$B_i^{tl} = \begin{bmatrix} \left(N_i\left(T_l(x) - T_l(x_i)\right)\right)_{,x} & 0 \\ 0 & \left(N_i\left(T_l(x) - T_l(x_i)\right)\right)_{,y} \\ \left(N_i\left(T_l(x) - T_l(x_i)\right)\right)_{,y} & \left(N_i\left(T_l(x) - T_l(x_i)\right)\right)_{,x} \end{bmatrix} \tag{3.46}$$

where B is the matrix of shape functions and $l = 1, 2, 3\ and\ 4$.

3.5.4 Level Set for Crack Propagation

The tracking of discontinuity motion in crack growth problems can be successfully achieved using a numerical tool known as level set method [22, 78]. This numerical method makes use of two orthogonal functions *i.e.*, normal level set function (ψ) and tangential level set function (φ). The work of the normal level set function is to track crack tip and the work of the tangential level set function is to track crack split/face, each time the crack path is updating. The values of these two level set functions are computed at nodes of the finite element mesh and are revised after every step of the crack propagation.

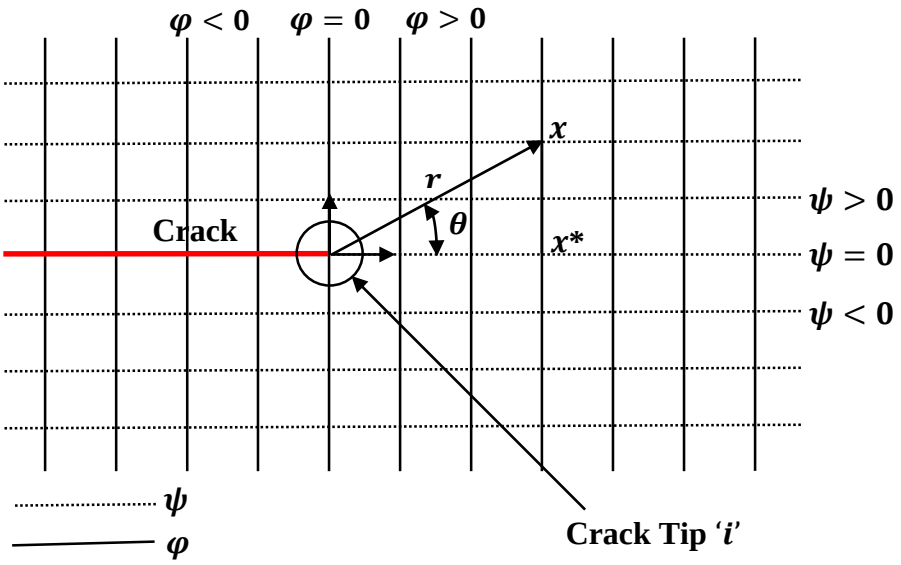

Figure 3.4: A 2D crack representation along with orthogonal level set functions

Figure 3.4 displays both the level set functions and provides a better understanding of the tracking operation being performed in the crack growth simulation. If $\varphi(x) < 0$, then the node corresponding to x lies behind the crack tip, $\varphi(x) > 0$ represents that the node is in front of crack tip and $\varphi(x) = 0$ represents that node lies on the crack tip. In a similar manner, if $\psi(x) < 0$, then the node corresponding to x lies below the crack path, $\psi(x) > 0$ represents that the node is lying above the crack path and $\psi(x) = 0$ represents that node lies on the crack path. The meeting point of the zero level set of ψ and the zero level set of φ provides the location of crack tip.

3.5.5 Numerical Integration

The numerical integration in XFEM has been performed using standard Gaussian quadrature. However the accuracy of the integration decreases at the regions *i.e.,* discontinuity along the crack and the singularity at the crack tip.

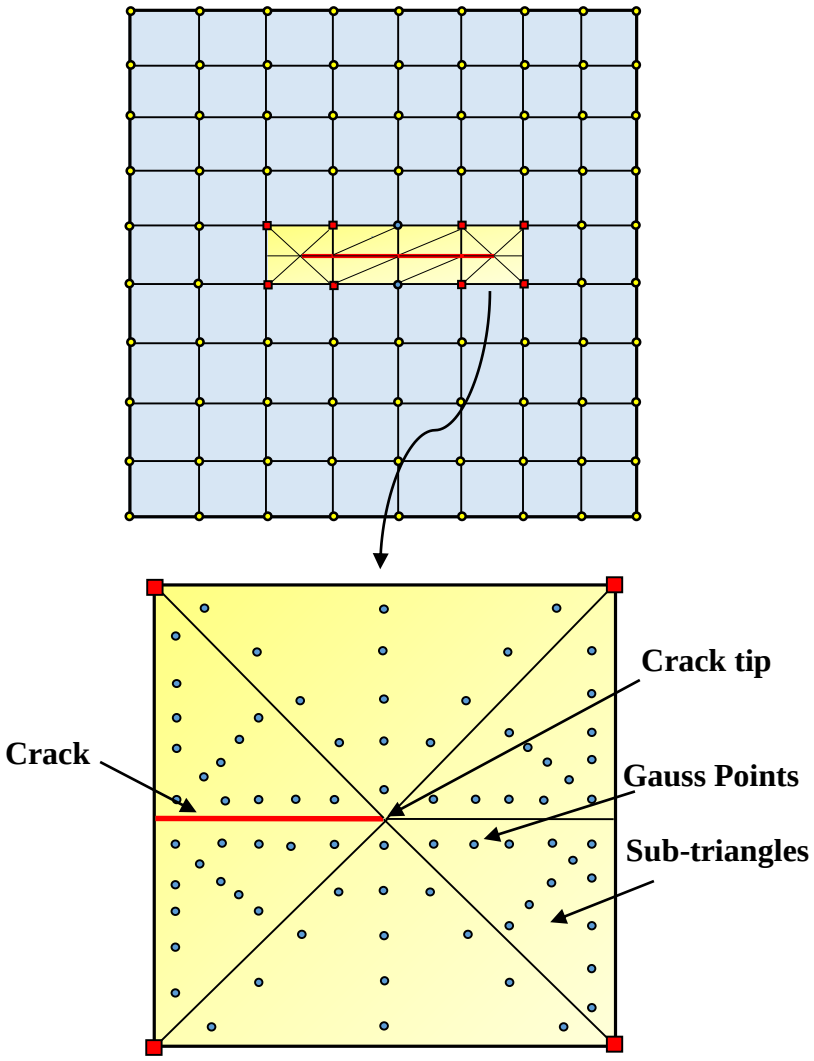

Figure 3.5: Sub-triangulation of the tip element for integration purpose

So to overcome this shortcoming, sub-triangulation technique has been used. In this approach, the elements which are intersected by the crack are sub-divided into sub-triangles which lead to more accurate results. Figure 3.5 illustrates the sub-triangulation in the crack split elements and crack tip elements. It must be taken into notice that due to singularity in the crack tip element, additional triangular sub-elements are required in elements containing the crack tip.

3.5.6 Evaluation of Stress Intensity Factors

Evaluation of individual SIFs (K_I, K_{II}) is done using the interaction integral approach and is a key part of the present work. Interaction integral approach is an effective method to compute the mixed-mode SIFs in which auxiliary stress-strain fields are superimposed into actual stress-strain fields [78, 79]. The interaction integral is obtained from the domain integral form of J-integral. J integral is a popular technique to compute the energy release rate in crack growth simulations [53]. In the equivalent domain integral approach, the contour integral is converted to an equivalent area integral (shown in Figure 3.6), simplifying its implementation in a finite element code [80]. The interaction integral in its equivalent area form, for both the equilibrium states for a cracked body can be written with the help of equation (3.47).

$$I^{(1,2)} = \int_A \left[\sigma_{ij}^1 \frac{\partial u_i^{(2)}}{\partial x_1} + \sigma_{ij}^2 \frac{\partial u_i^{(1)}}{\partial x_1} - W^{(1,2)}\delta_{1j}\right]\frac{\partial q}{\partial x_j} dA \tag{3.47}$$

where q represents a weighting function; δ_{1j} represents the Kronecker delta function; $W^{(1,2)}$represents the interaction work and 1,2 represents the independent actual state and auxiliary state.

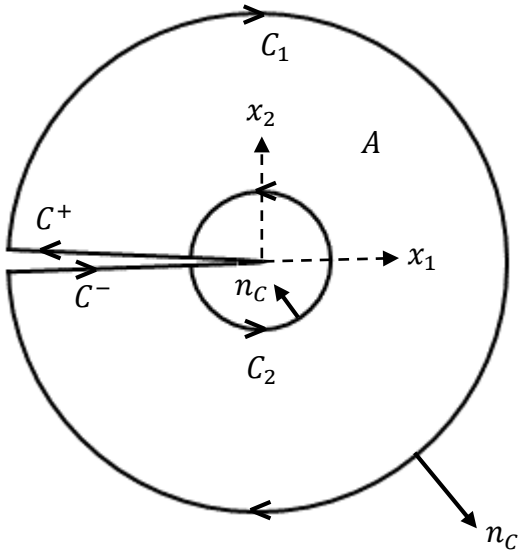

Figure 3.6: Domain of J-integral in its equivalent area form

The relation for the interaction strain energy is given by equation (3.48).

$$W^{(1,2)} = \frac{1}{2}\left(\sigma_{ij}^{(1)}\varepsilon_{ij}^{(2)} + \sigma_{ij}^{(2)}\varepsilon_{ij}^{(1)}\right) = \sigma_{ij}^{(1)}\varepsilon_{ij}^{(2)} = \sigma_{ij}^{(2)}\varepsilon_{ij}^{(1)} \tag{3.48}$$

where σ_{ij} represents the stress field and ε_{ij} represents the strain field. The individual stress intensity factors can be extracted using equation (3.49).

$$I^{(1,2)} = \frac{2}{E'}\left(K_I^{(1)}K_I^{(2)} + K_{II}^{(1)}K_{II}^{(2)}\right) \tag{3.49}$$

The use of weighting function is the transformation of contour integral form of interaction integral to an equivalent domain form. It has a value of one at crack tip and zero on the contour. When applying the interaction integral approach in a finite element code, a virtual circle of a specified radius is taken into consideration around the crack tip. The virtual circle (shown by figure 3.7) represents the domain of J-integral and the numerical integration using Gaussian quadrature rule is performed only on those elements which are either crossed by the circle or are lying inside the circle. The radius of the circle is calculated on the basis of characteristic length of crack tip element [81]. In a two dimensional case, the characteristic length will be equal to the square root of tip element area. The radius of the circle is taken as thrice the characteristic length of the tip element. The weighting function q will have value of unity for all those nodes lying inside the J-domain circle, and a value of zero for the nodes lying outside the circle. The values of the weighting function are then interpolated within the elements with the help of shape functions, as given by equation (3.50).

$$\mathrm{q} = \sum_{i=1}^{n} N_i\,(x)\mathrm{q}_i \tag{3.50}$$

where q_i represents the value of the weighting function corresponding to the nodes of the elements lying inside J-domain circle or crossing it.

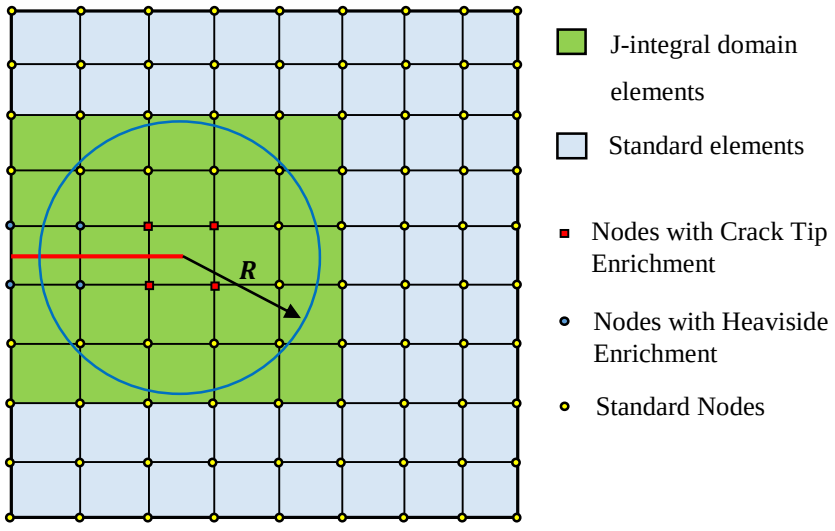

Figure 3.7: Computation of Stress intensity factors using J-integral domain

The equation of interaction integral given in equation (3.47) can be expressed more clearly in terms of Gaussian quadrature integration rule over an element with the help of equation (3.51).

$$I^{(1,2)} = \sum_{m=1}^{N^G} \left\{ \left[\sigma_{ij}^1 \frac{\partial u_i^{(2)}}{\partial x_1} + \sigma_{ij}^2 \frac{\partial u_i^{(1)}}{\partial x_1} - W^{(1,2)} \delta_{1j} \right] \frac{\partial q}{\partial x_j} \right\} w_m \det J \tag{3.51}$$

where N^G represents the total number of Gaussian points associated with a particular element; w_m are the weights corresponding to Gaussian points; and J represents the Jacobian matrix.

3.5.7 Crack Growth

For the simulation purpose, a fixed predetermined value for crack growth, Δl is provided as the input parameter. As the part of first step, discrete equations are solved for unknown displacement, stress and strain fields. Then in the second step, the mixed mode SIFs are computed at the crack tip using the equation (3.49), for each step of crack growth. The range of SIFs for a constant amplitude loading is provided by the equation (3.52).

$$\Delta K = K_{max} - K_{min} \tag{3.52}$$

where, K_{max} is computed corresponding to maximum applied load and K_{min} is computed corresponding to minimum applied load.

In the present work, direction of crack growth in XFEM simulation has been achieved with the help of maximum tensile stress principle. This crack growth criterion states the direction of crack growth perpendicular to maximum tension in the material. The values for equivalent mode I stress intensity factor and crack growth direction θ_c is estimated using the equation (3.53) and (3.54).

$$\Delta K_{Ieq} = \Delta K_I \left(\cos\left(\frac{\theta_c}{2}\right) \right)^3 - 3\Delta K_{II} \left(\cos\left(\frac{\theta_c}{2}\right) \right)^2 \sin\left(\frac{\theta_c}{2}\right) \tag{3.53}$$

$$\theta_c = 2 \tan^{-1} \left(\frac{K_I \pm \sqrt{{K_I}^2 + 8{K_{II}}^2}}{4K_{II}} \right) \tag{3.54}$$

The failure of the structure under consideration will occur, whenever $(K_{Ieq})_{max} > K_{IC}$. The equivalent value of the SIF $(K_{Ieq})_{max}$ is obtained in case of maximum loading situation and K_{IC} is the fracture toughness of the material.

3.5.8 Implementation in Finite Element Code

The implementation of the numerical XFEM approach in a computerized finite element code can be illustrated with the help of the flowchart given in Figure 3.8.

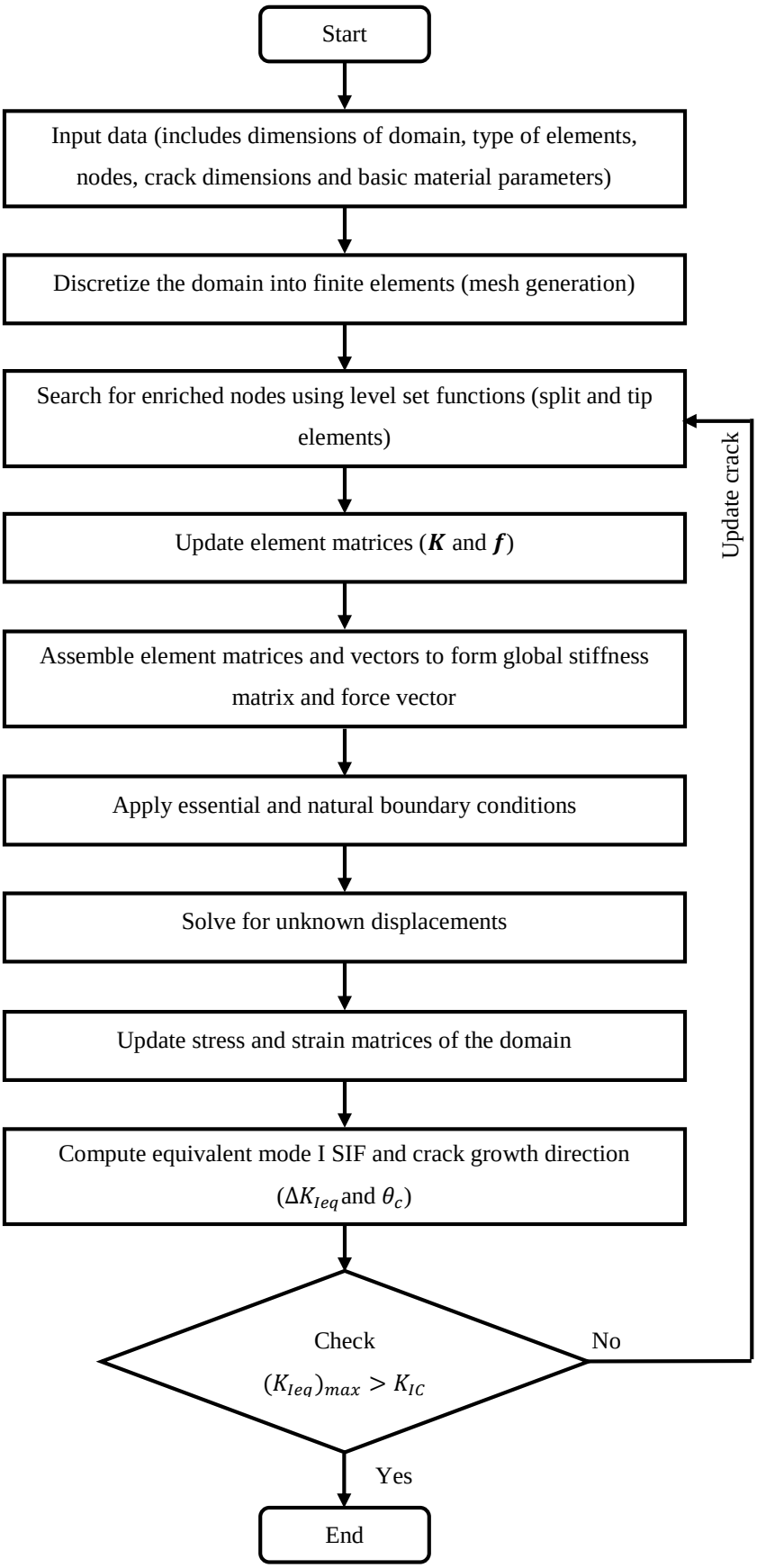

Figure 3.8: Flowchart of XFEM to simulate crack growth

Chapter 4

Numerical Results and Discussion

In the present work, the crack growth in a thin plate has been simulated using XFEM. For the crack growth analysis, two cases have been considered i.e., thin plate containing an edge crack and thin plate containing a centre crack. Both of these thin plates are subjected to external cyclic loading. The plate considered for crack growth analysis is made up of CNT reinforced polymer nanocomposite. For the crack growth simulation, it is considered to be homogenous in nature. The equivalent properties of the plate have been computed by varying the percentage of CNT from 0 to 4 % by weight in the polymer matrix. A plate of size 100 mm × 200 mm has been considered for the simulation purpose. Mode I fracture and plane stress condition has been assumed for the crack growth analysis. The plate is subjected to cyclic tensile load varying from σ_{min}= 0 MPa to σ_{max} = 3.65 MPa at the top edge. The bottom edge of the plate is constrained in the y direction. A maximum increment of 2 mm per step has been set for crack growth until the failure of the plate. The SIF values are calculated at each stage of crack growth till it exceeds the SIF value of the plate. A higher order Gauss quadrature has been used for the integration purpose. For the elements containing a discontinuity, sub-triangulation technique has been used for integration. The six and four sub-triangles are considered for tip element and split element respectively. A total of 13 Gaussian points have been taken for each sub-triangle in the tip element and 3 Gaussian points in each sub-triangle in the split element.

Serial No.	Mesh Size	Stress Intensity Factor (SIF)
1	25 × 50	16.1598
2	30 × 60	15.8581
3	35 × 70	15.7752
4	40 × 80	15.8870
5	45 × 90	15.9088

Table 4.1: Convergence study for a thin plate containing an edge crack

A convergence study has also been performed for the edge cracked plate subjected to fatigue loading using a set of different set of mesh sizes. Based on the values obtained for SIF using different set of mesh sizes (shown in Table 4.1 and Figure 4.1), it has been estimated that the solution converges at a mesh size of 40 × 80. Therefore, the domain has been discretized

into 3081 four node quadrilateral elements with a uniform mesh size of 40 × 80 nodes in x and y directions for the crack growth simulation in the forthcoming analysis.

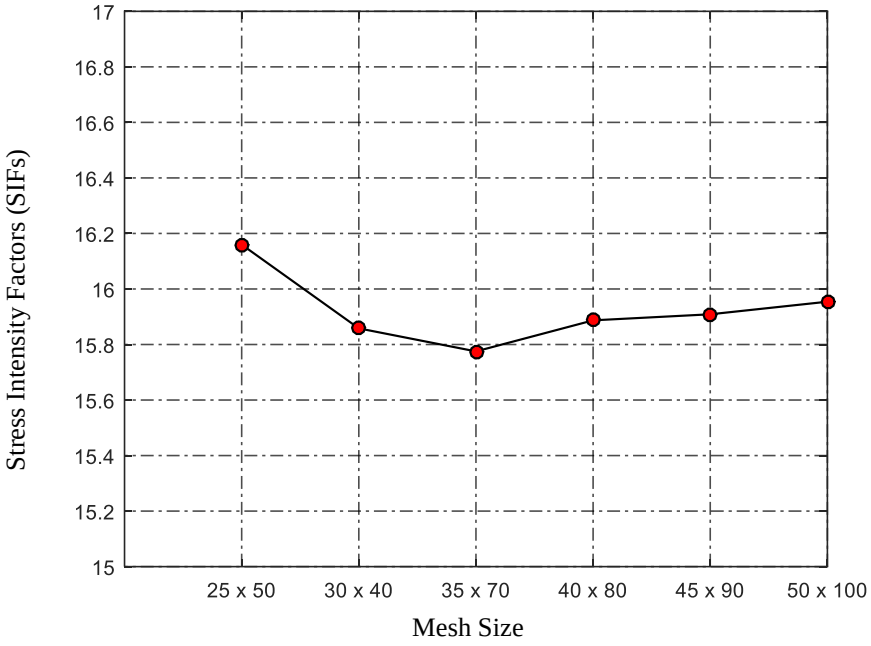

Figure 4.1: SIFs corresponding to different mesh sizes for a thin plate containing an edge crack

4.1 Evaluation of Equivalent Properties

The equivalent properties of the nanocomposite play a major role in crack growth as the thin plate is considered to be homogeneous in composition. The properties of epoxy have been considered for the polymer matrix. Since the CNT and epoxy matrix have their own properties, there is a need to calculate the equivalent properties for the resultant nanocomposite. The equivalent homogenous material is shown in Figure 4.2. In this work, the equivalent properties of the nanocomposite have been computed by varying the CNT content in the polymer matrix. The equivalent properties comprises elastic modulus, Poisson's ratio, fracture energy and fracture toughness. For the computation of equivalent properties, both SWCNTs and MWCNTs have been taken as the reinforcements in the polymer matrix. The aspect ratio of SWCNT and MWCNT has been kept same for the comparison purpose. The crack growth simulation has been done separately for both SWCNT reinforced nanocomposite and MWCNT reinforced nanocomposite. The elastic modulus of the nanocomposite has been evaluated using modified Halpin-Tsai equation. The weight fraction has been converted to volume fraction using rules of mixture. Similarly, the Poisson's ratio has been evaluated using the rules of mixture. The fracture energy has been evaluated considering the CNT pull-out and CNT debonding as the

main toughening criteria. Fracture energy and fracture toughness have been computed based on the equations (3.20) and (3.22).

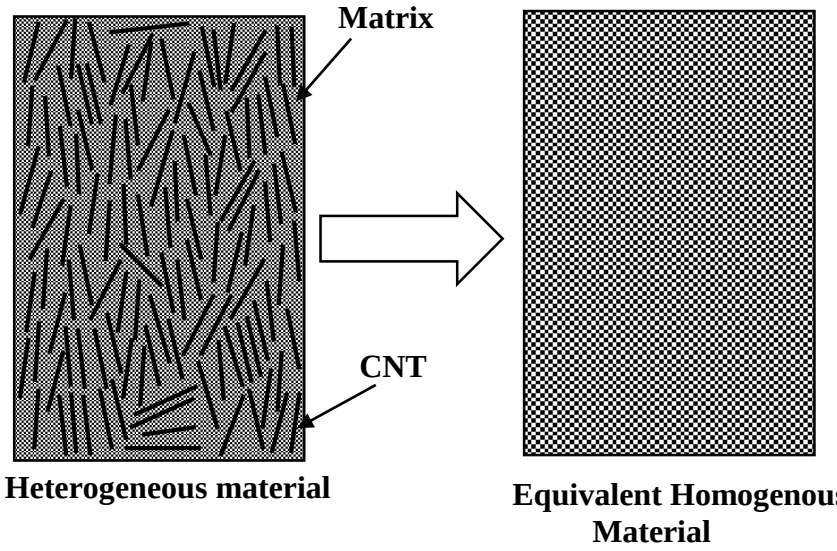

Figure 4.2: Equivalent properties evaluation

The geometric and material properties of the constituents of nanocomposite used for the evaluation of equivalent properties are given in table 4.2.

Name	Symbol	Unit	Value
Density of CNT	ρ_{NT}	kg/m^3	1800
Graphite layer thickness	t	nm	0.34
Poisson's ratio of CNT	ν_{NT}		0.16
Single Walled Carbon Nanotube(SWCNT)			
Length	l_{NT}	nm	322.32
Diameter	d_{NT}	nm	1.36
Elastic modulus	E_{NT}	GPa	1002
Strength	σ_{NT}	GPa	30
Multi-walled Carbon Nanotube(MWCNT)			
Length	l_{NT}	µm	3.08
Diameter	d_{NT}	nm	13
Elastic modulus	E_{NT}	GPa	470
Strength	σ_{NT}	GPa	28
Epoxy Properties			
Density	ρ_m	kg/m^3	1200
Elastic modulus	E_m	GPa	2.90

Fracture energy	G_{CU}	J/m^2	133
Interfacial fracture energy	G_i	J/m^2	25
Interfacial strength	τ_i	MPa	47
Poisson's ratio	ν		0.35

Table 4.2: Material parameters used in mathematical modelling [6, 11, 43]

4.1.1 Elastic Modulus

The elastic modulus has been evaluated using the modified Halpin-Tsai equations which attribute elastic modulus in both the longitudinal and transverse direction. Since the Halpin-Tsai equation uses the CNT volume fraction, the weight fraction has been converted to volume fraction using rules of mixture. The elastic modulus of the modified nanocomposite has been evaluated taking SWCNTs and MWCNTs as the separate reinforcements inside the epoxy matrix. The content of CNTs has been varied up to 4 % by weight in the epoxy matrix taking different factors into account [1, 7, 82]. The rules of mixture are employed to convert the weight fraction of CNT in to the volume fraction to estimate the elastic modulus.

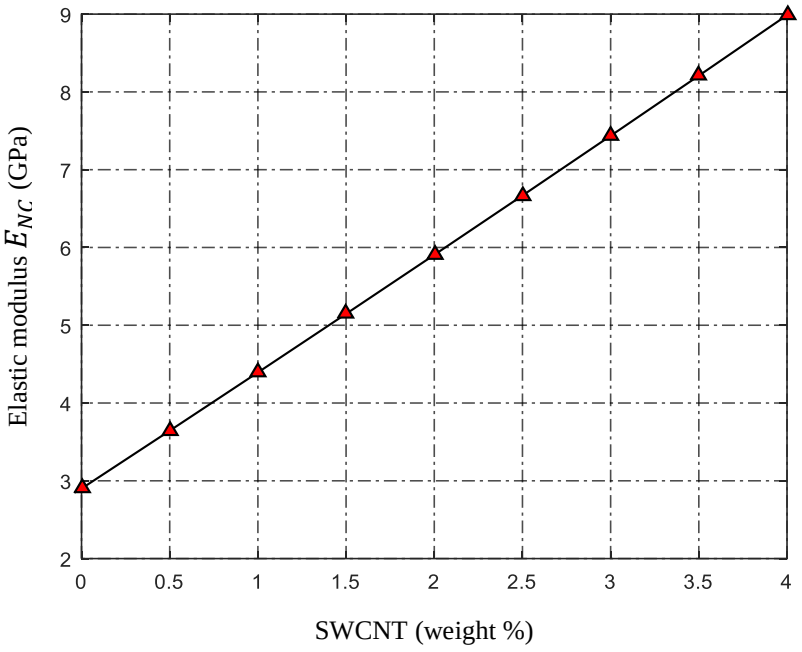

Figure 4.3: Influence of SWCNT content on the elastic modulus of modified epoxy nanocomposite

Figure 4.3 and Figure 4.4 shows the influence of variation of SWCNT and MWCNT content on the elastic modulus of modified epoxy nanocomposites respectively. It can be clearly perceived from Figure 4.3 and 4.4 that there is a linear increase in elastic modulus of the subsequent nanocomposite with respect to increase in weight of CNT in the epoxy matrix.

Moreover, the rate of this increment is higher for SWCNT nanocomposites as compared to MWCNT nanocomposites. It should be noted that the CNTs have been considered to be taking part in the load transfer mechanism, and hence in case of MWCNTs, only the outer layer is taking part in the load transfer mechanism.

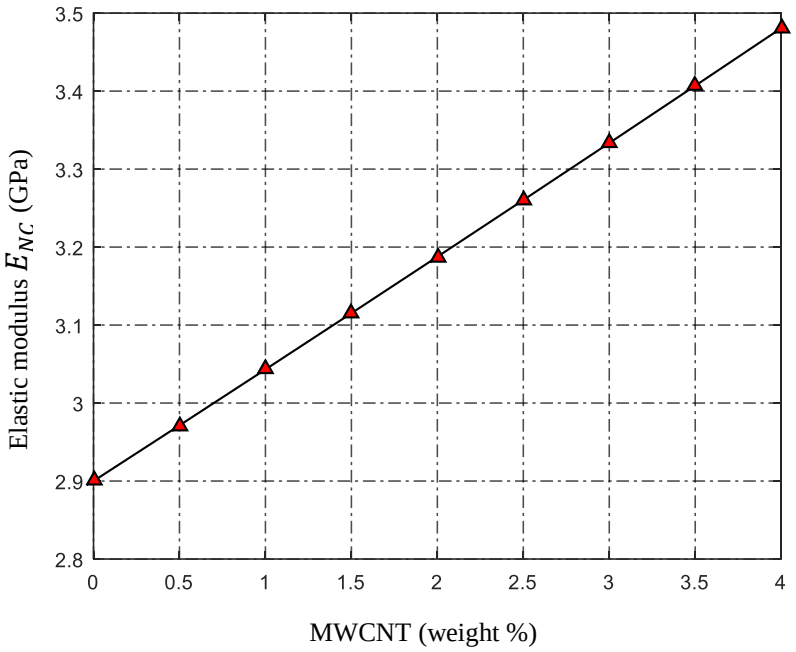

Figure 4.4: Influence of MWCNT content on the elastic modulus of modified epoxy nanocomposite

4.2 Fracture Energy

Fracture energy has been computed using equation (3.20) which is the summation of fracture energy of unmodified epoxy polymer and the contributing fracture mechanisms such as CNT pull out, debonding and rupture. Figure 4.5 illustrates the influence of SWCNTs % by weight on the fracture energy of modified epoxy nanocomposite. Figure 4.6 illustrates the influence of aspect ratio on the fracture energy of modified epoxy nanocomposite, for different content of SWCNT % by weight. The aspect ratio ($l_{NT} \ / \ d_{NT}$) values ranges from 200 to 1000. Similarly, Figure 4.7 and 4.8 illustrates the influence of variation in % by weight and aspect ratio of MWCNTs on the fracture energy of modified epoxy nanocomposite.

Based on the graphs, a clear observation can be made that there is an increase in fracture energy with the increase of CNTs content inside the polymer matrix. This is due to the assumption that all CNTs are taking part in the contributing fracture mechanisms. It can be also seen that the fracture energy is improving by increasing the aspect ratio of CNTs. Since, aspect ratio of the CNT depends on the length and diameter of the CNT, they as well are the important parameters responsible for the increase in fracture energy. It can be concluded that the fracture

energy of the modified epoxy nanocomposite is rising with increase in length of the CNTs. Similarly, the fracture energy of the modified epoxy nanocomposite is rising with the reduction in diameter of the CNTs.

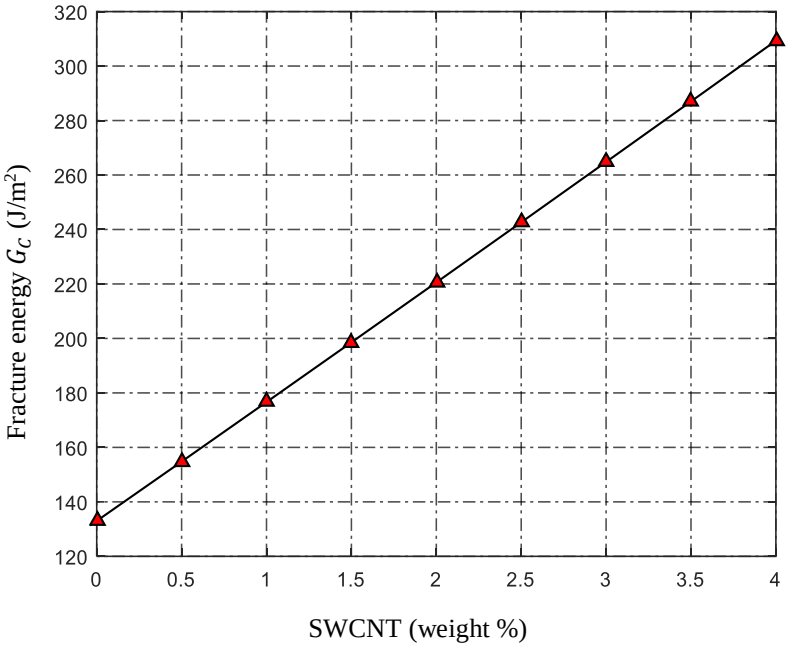

Figure 4.5: Influence of SWCNT content on the fracture energy of modified epoxy nanocomposite

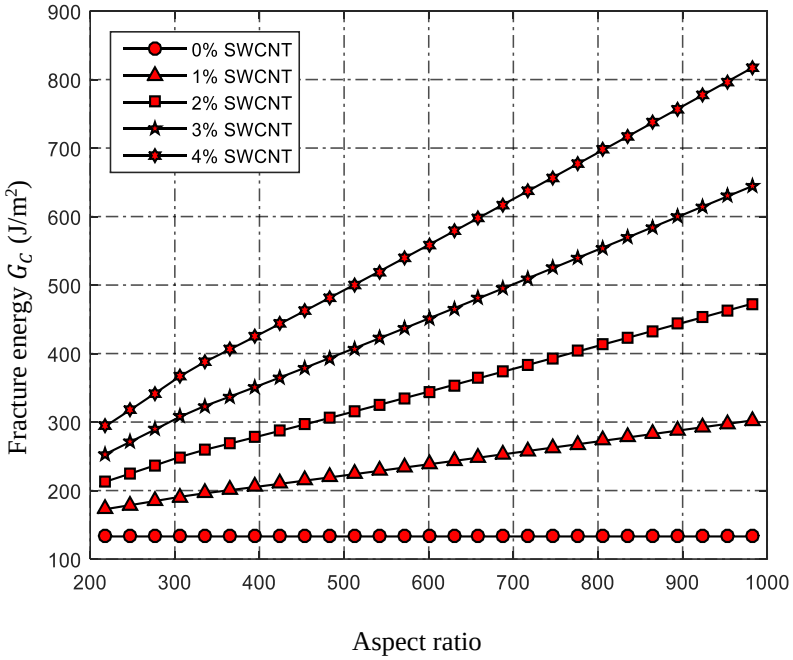

Figure 4.6: Effect of aspect ratio on the fracture energy for different SWCNT content in modified epoxy nanocomposite

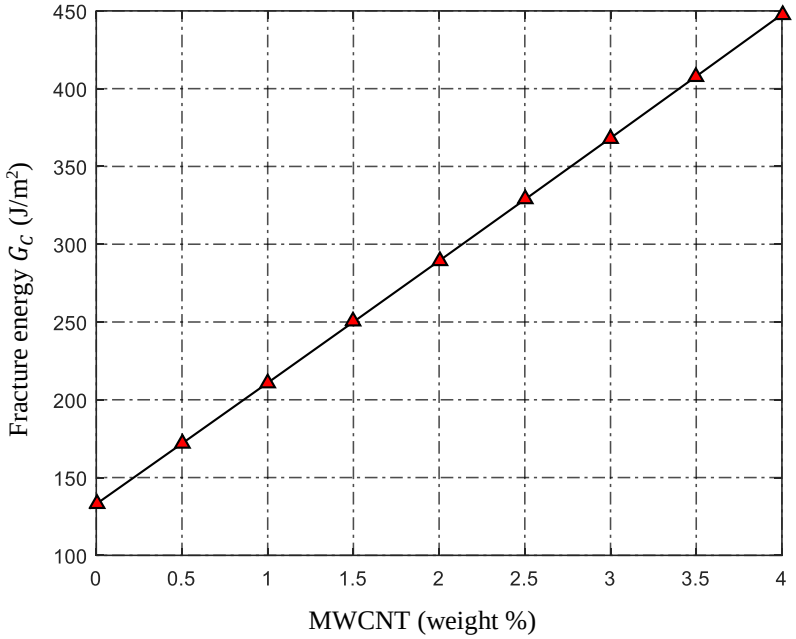

Figure 4.7: Influence of MWCNT content on fracture energy of modified epoxy nanocomposite

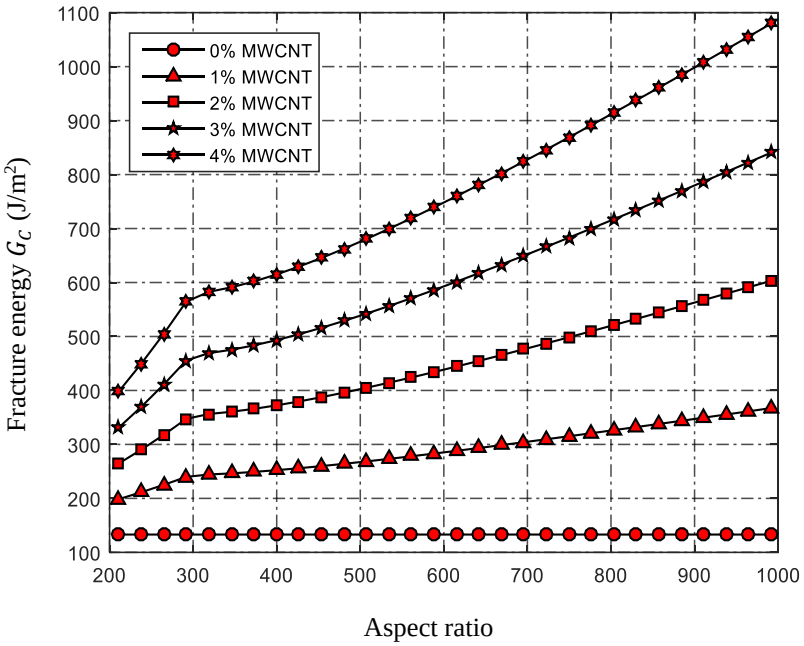

Figure 4.8: Effect of aspect ratio on the fracture energy for different MWCNT content in modified epoxy nanocomposite

4.2.1 Fracture Toughness

The fracture toughness is the most important parameter in the numerical crack growth simulation and is usually termed as critical stress intensity factor. Higher the fracture toughness value, more time it will take for the failure of the component. In the present work, the relation

between fracture toughness and fracture energy is given by equation (3.22). Figure 4.9 illustrates the influence of SWCNTs % by weight on the fracture toughness of modified epoxy nanocomposite. Figure 4.10 illustrates the influence of aspect ratio on the fracture toughness of modified epoxy nanocomposite with the variation in % by weight of SWCNTs in the epoxy matrix.

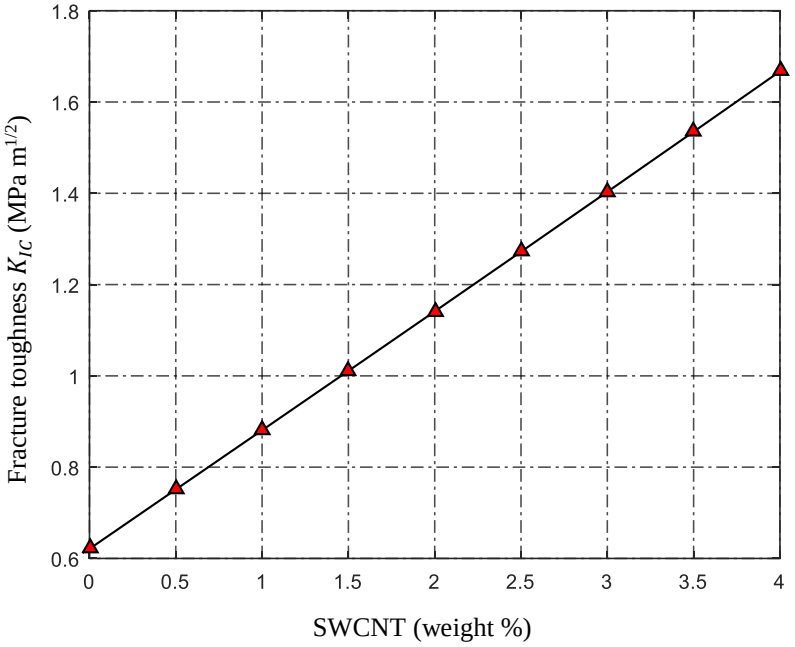

Figure 4.9: Influence of SWCNT content on the fracture toughness of modified epoxy nanocomposite

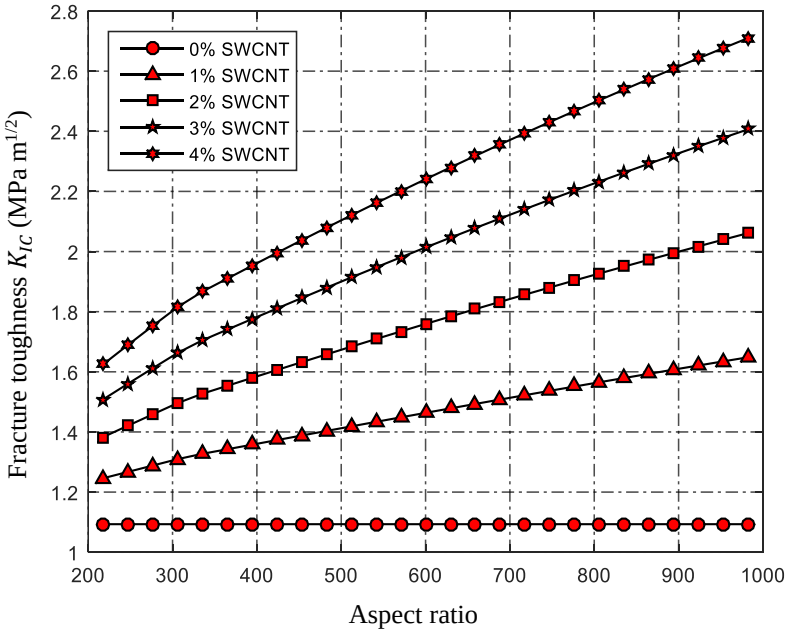

Figure 4.10: Effect of aspect ratio on fracture toughness for different content of SWCNT in modified epoxy nanocomposite

Similarly, Figure 4.11 and 4.12 illustrates the influence of variation in % by weight and aspect ratio of MWCNTs on the fracture toughness of modified epoxy nanocomposite respectively.

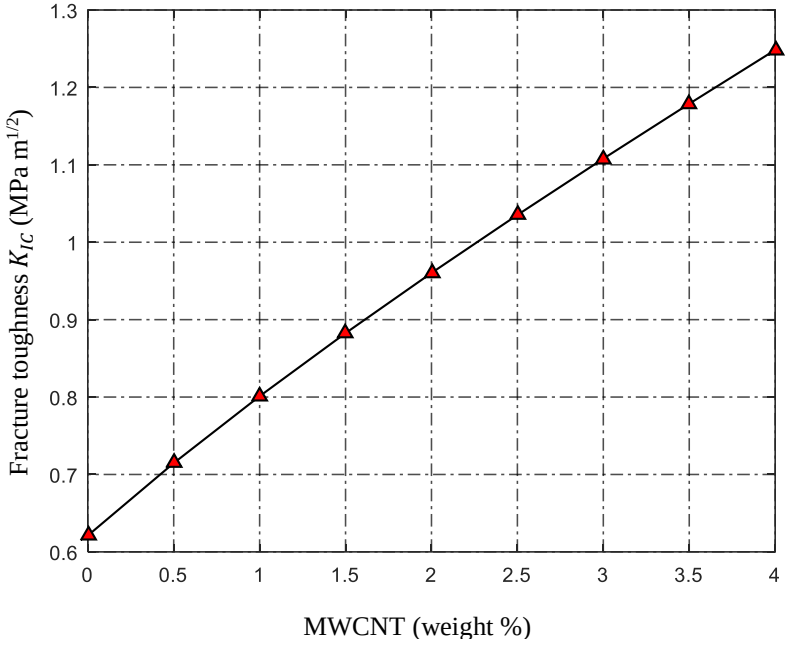

Figure 4.11: Influence of MWCNT content on the fracture toughness of modified epoxy nanocomposite

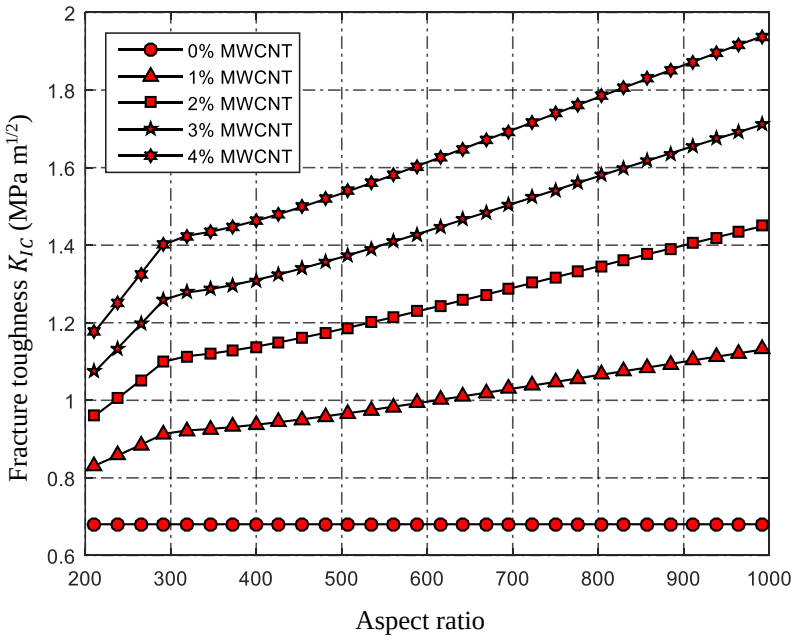

Figure 4.12: Effect of aspect ratio on fracture toughness for different content of MWCNT in modified epoxy nanocomposite

The observations for the fracture toughness are similar to those of fracture energy. There is an improvement in fracture toughness with the increase in aspect ratio of SWCNTs and MWCNTs in the modified epoxy nanocomposite. As the fracture toughness plays a vital role in crack growth analysis of different structures, improvement in the fracture toughness values will certainly result in an enhanced life of the component. In addition, using CNTs with higher aspect ratios will result in improved fracture toughness values.

4.3 Crack Growth Analysis

For the crack growth analysis, the following two cases have been considered (i) A thin plate containing an edge crack subjected to cyclic load (shown in Figure 4.13) and (ii) A thin plate containing a centre crack subjected to cyclic load (shown in Figure 4.14). In both the cases, crack growth analysis has been done separately taking SWCNTs and MWCNTs as the reinforcements. The % content of SWCNTs and MWCNTs by weight has been varied from 0 to 4 % in the polymer matrix of the nanocomposite. Before the crack growth analysis, a comparison study has also been performed for the validation of numerical results obtained using XFEM. For this study, theoretical stress intensity factors have been computed using the analytical relation for edge cracked plate and centrally cracked plate.

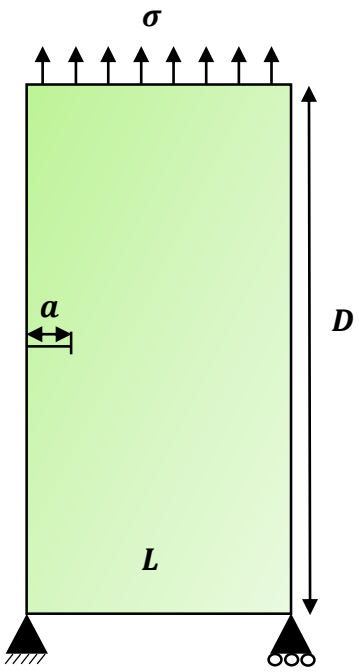

Figure 4.13: Case (i): Thin plate containing an edge crack subjected to cyclic tensile load on the top edge

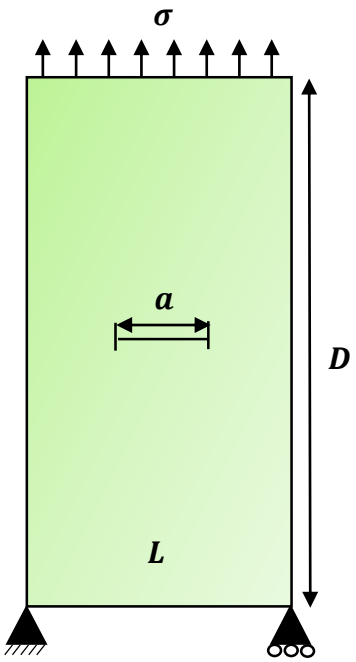

Figure 4.14: Case (ii): Thin plate containing a centre crack subjected to cyclic tensile load on the top edge

The SIF values [53] for the thin plate containing an edge crack is calculated using the analytical relation provided in equation (4.1)

$$K_{IC} = C_1 \sigma \sqrt{\pi a} \tag{4.1}$$

where,

$$C_1 = [1.12 - 0.23(a/L) + 10.6(a/L)^2 - 21.7(a/L)^3 + 30.4(a/L)^4] \tag{4.2}$$

Similarly, the SIF values [53] for the thin plate containing a centre crack is calculated using the analytical relation given in equation (4.3)

$$K_{IC} = C_2 \sigma \sqrt{\pi (a/2)} \tag{4.3}$$

where,

$$C_2 = [1 + 0.128(a/L) - 0.288(a/L)^2 + 1.523(a/L)^3] \tag{4.4}$$

In equation (4.4), a represents the length of the crack; L represents the length of the rectangular plate; and σ represents the cyclic tensile load.

In order to conduct the comparative study, the SIF values have been computed using XFEM formulation for a cyclic load varying from σ_{min}= 0 MPa to σ_{max} = 2 MPa. The crack length for edge crack is 5 mm and crack length for the centre crack is 10 mm respectively. The equivalent properties of the plate corresponding to CNT content of 0 % by weight in the matrix has been considered for the simulation purpose.

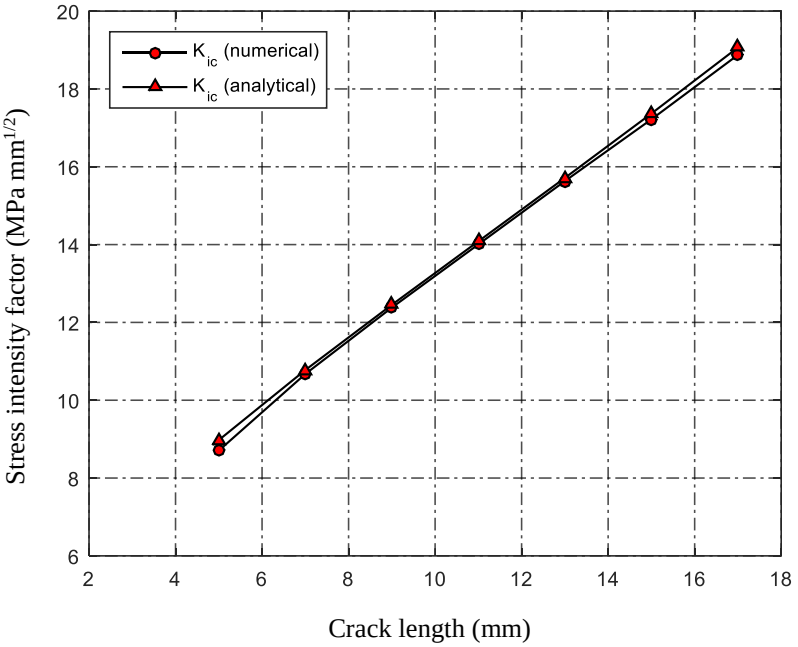

Figure 4.15: Comparative study for a thin plate containing an edge crack

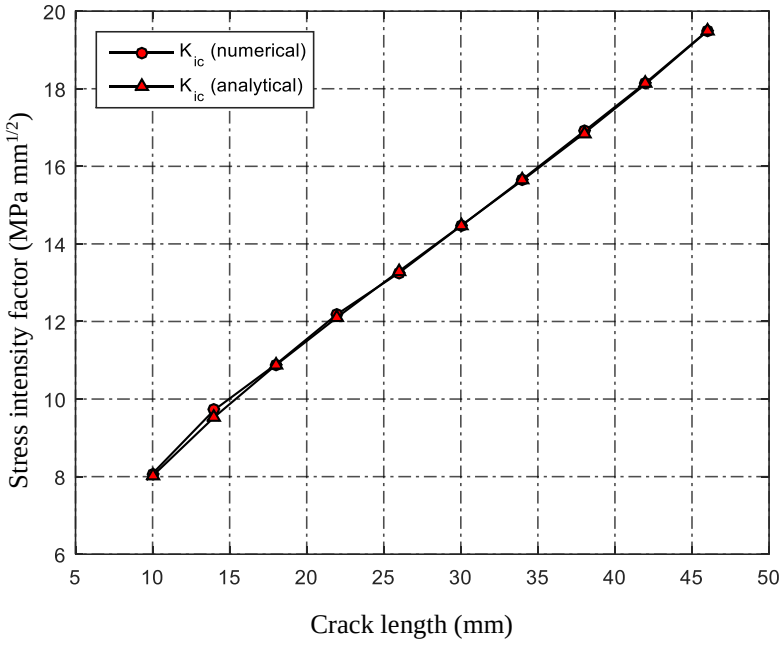

Figure 4.16: Comparative study for a thin plate containing a centre crack

Figure 4.15 and 4.16 presents the comparison between numerical and analytical results for both the thin plate containing an edge crack and a centre crack. The error in SIF values for the edge crack plate are found to be 3.01, 0.94, 0.58, 0.56, 0.52, 0.85 and 1.01 % for 5, 7, 9, 11, 13, 15 and 17 mm crack length respectively. Similarly, the error in the SIF values for centre

crack plate are found to be 0.79, 1.94, 0.18, 0.66, 0.33, 0.04, 0.17, 0.3, 0.17 and 0.04 % for 10, 14, 18, 22, 26, 30, 34, 38, 42 and 46 mm crack length respectively.

4.3.1 Case I: Thin plate containing an Edge Crack subjected to Cyclic Tensile Loading

A thin rectangular plate having dimensions of 100 mm × 200 mm containing an edge crack is considered, shown in Figure 4.13, for the crack growth simulation without any other discontinuity. The edge crack is having an initial length of 5 mm for the crack growth simulation. A cyclic tensile load ranging between σ_{min}= 0 MPa to σ_{max} = 3.65 MPa is applied on the top edge of the rectangular plate. The bottom edge of the plate is fixed *i.e.* constrained in the y direction. The domain of the rectangular plate is discretized into 3081 number of 4-noded quadrilateral elements, with a uniform mesh size of 40 × 80 nodes, in both x and y directions (shown in Figure 4.17). A fixed crack growth Δl of 2 mm has been taken for the simulation purpose.

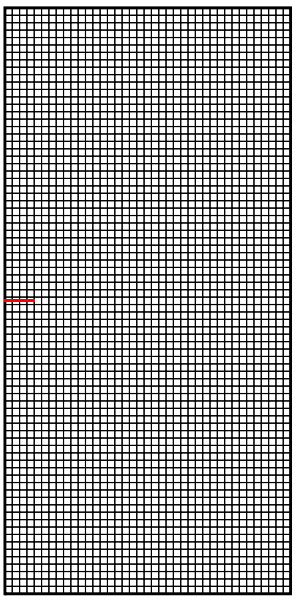

Figure 4.17: Rectangular plate mesh of 40 × 80 nodes containing an edge crack

The SIF values obtained by XFEM simulation for both SWCNT reinforced nanocomposite and MWCNT reinforced nanocomposite are presented in Figure 4.18 and 4.19 respectively. The SIF values are evaluated for each step of crack propagation and are compared with the fracture toughness of the plate. The thin edge cracked plate fails once the SIF value exceeds the fracture toughness of the plate. The fracture toughness values corresponding to different content of CNT (SWCNT and MWCNT) by weight in the epoxy matrix have been used in the numerical simulation.

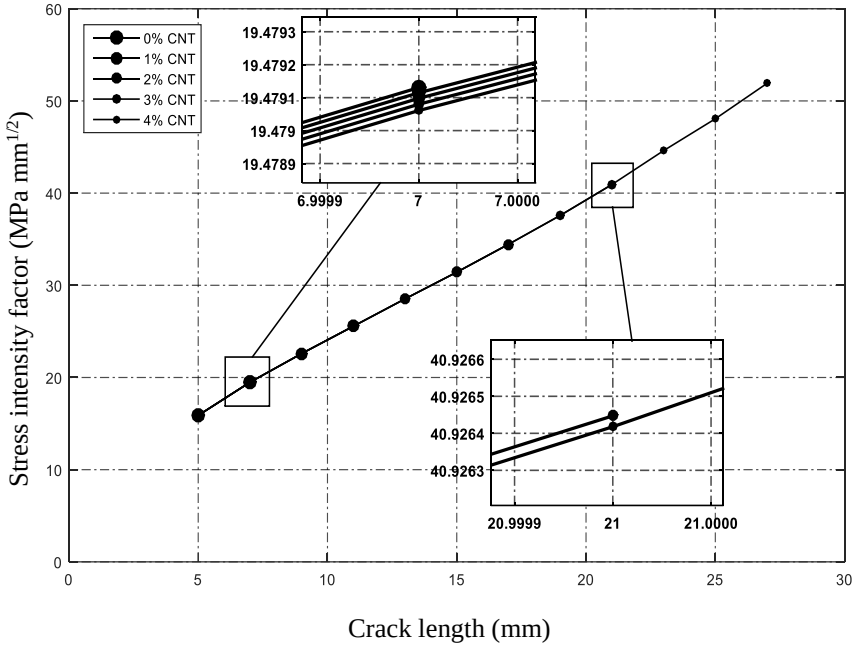

Figure 4.18: Effect of crack length on SIF for different content of SWCNT in modified epoxy nanocomposite plate containing an edge crack

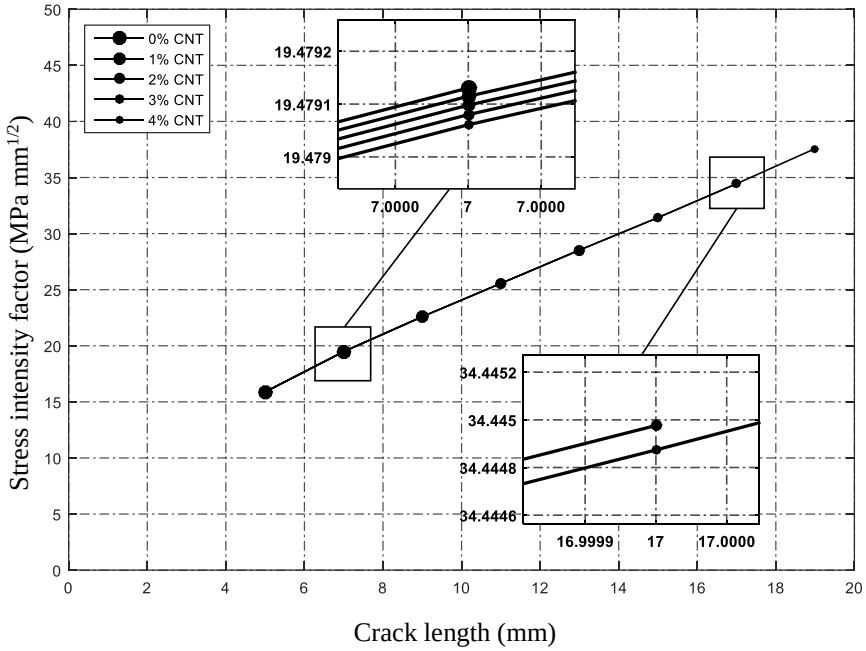

Figure 4.19: Effect of crack length on SIF for different content of MWCNT in modified epoxy nanocomposite plate containing an edge crack

A crack extension of 6, 12, 16, 22 mm is observed for the edge cracked plate corresponding to 1, 2, 3 and 4 % by weight content of SWCNT in the epoxy matrix. Similarly, a crack extension of 4, 8, 12, 14 mm is observed for the edge cracked plate corresponding to 1,

2, 3 and 4 % by weight content of MWCNT in the epoxy matrix. In comparison to these values, a crack extension of only 2 mm is observed for the thin nanocomposite plate containing 0 % by weight content of CNT in the polymer matrix. Since, higher values of crack extension are being observed as the wt. % of CNT is increasing within the polymer matrix, it can be concluded that the life of the thin plate is also getting increased.

4.3.2 Case II: Thin plate containing a Centre Crack subjected to Cyclic Tensile Loading

A thin rectangular plate having dimensions of 100 mm × 200 mm containing a centre crack, shown in Figure 4.14, is considered for the simulation purpose. The length of the centre crack is taken to be 10 mm, twice the length of an edge crack. A cyclic tensile load ranging between σ_{min}= 0 MPa to σ_{max} = 3.65 MPa is applied on the uppermost edge of the rectangular plate. The lowermost edge of the plate is fixed *i.e.* constrained in the y direction. The domain of the rectangular plate is discretized into 3081 number of 4-noded quadrilateral elements, with a uniform mesh size of 40 × 80 nodes, in both x and y directions (shown in Figure 4.20). A fixed crack growth of 2 mm for both the crack tips has been taken for the simulation purpose. Hence, a total crack extension of 4 mm is taking place after each step of crack propagation. The SIF values obtained by XFEM simulation for both SWCNT reinforced nanocomposite and MWCNT reinforced nanocomposite are presented in Figure 4.21 and 4.22.

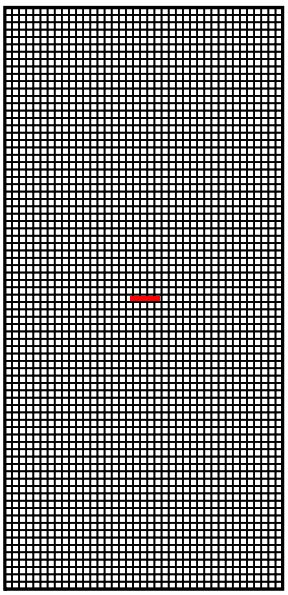

Figure 4.20: Rectangular plate mesh of 40 × 80 nodes containing an centre crack

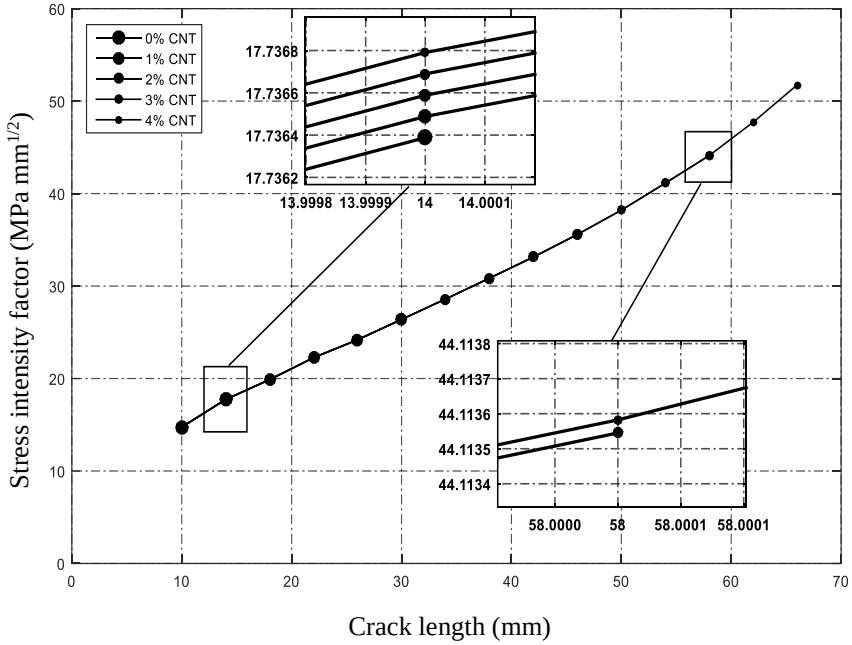

Figure 4.21: Effect of crack length on SIF for different content of SWCNT in modified epoxy nanocomposite plate containing a centre crack

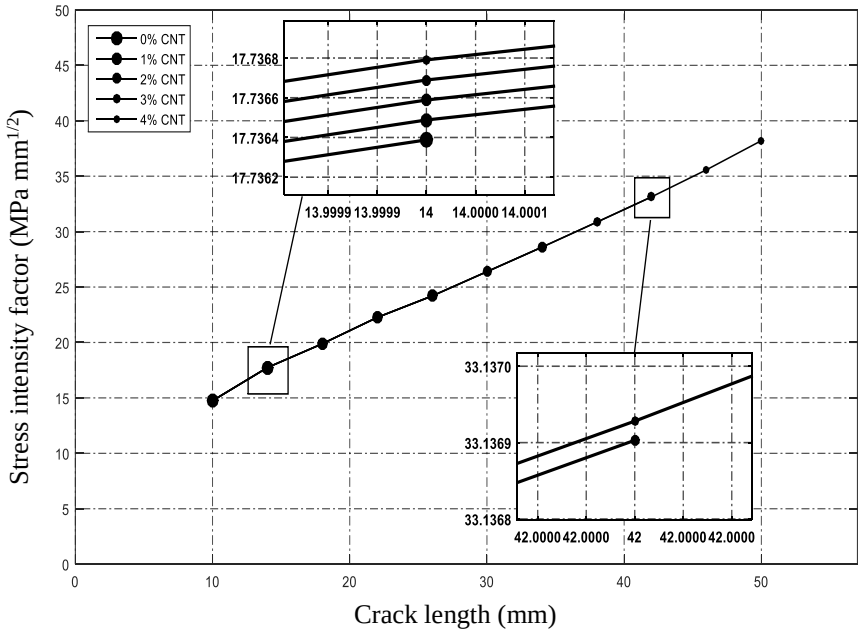

Figure 4.22: Effect of crack length on SIF for different content of MWCNT in modified epoxy nanocomposite plate containing a centre crack

The SIF values are evaluated for each step of crack propagation and are compared with the fracture toughness value of the plate. In the present case of a centre crack, the SIF values are calculated at both the crack the tips. The SIF value whichever is higher is taken as the failure parameter among the mutually calculated SIF values at both the crack tips. The thin plate fails,

once the calculated SIF value exceeds the fracture toughness value of the plate. The fracture toughness values corresponding to different content of CNT (SWCNT and MWCNT) by weight in the epoxy matrix have been used in the numerical simulation. A crack extension of 20, 36, 48 and 56 mm is observed for the centre cracked plate corresponding to 1, 2, 3 and 4 % by weight content of SWCNT in the epoxy matrix. Similarly, a crack extension of 16, 24, 32 and 40 mm is observed for the centre cracked plate corresponding to 1, 2, 3 and 4 % by weight content of MWCNT in the epoxy matrix. In comparison to these results, a crack extension of only 4 mm is observed for the thin nanocomposite plate containing 0 % by weight content of CNT in the epoxy matrix. Since, higher values of crack extension are being observed as the wt. % of CNT is increasing within the polymer matrix, it can be concluded that the life of the thin plate is also getting increased.

Chapter 5

Conclusions

CNT reinforced polymer nanocomposites possess decent mechanical properties which can prove to be vital in applications where lower weight and higher stiffness is required. As reinforcement of CNT in the polymer matrix is still not in the mature stage due to several issues regarding processing of nanocomposites, assessment of the mechanical properties of these nanocomposites will certainly benefit in their sustainable development. Enhancement in the fracture toughness values of polymer matrix due to addition of CNT as the reinforcement is an important part of this study. Improvement in fracture toughness values of the nanocomposite will lead to their higher life expectancy which can be advantageous in applications involving cyclic loads. In the present work, XFEM has been utilized for the crack growth simulation in a thin rectangular plate containing an edge crack and a centre crack. For the crack growth simulation, the equivalent properties of the CNT reinforced polymer nanocomposite have been chosen as the input modelling parameters. The equivalent properties have been evaluated by varying the % by weight content of CNT up to 4 % in the polymer matrix of the nanocomposite. An improvement in elastic modulus is observed when the SWCNT and MWCNT weight content is increased inside the epoxy matrix. On the basis of present simulations, the following conclusions are drawn:

- The elastic modulus of the nanocomposite is increased by 210 %, when the weight content of SWCNT is increased from 0 to 4 % by weight within the epoxy matrix. Similarly, the elastic modulus is increased by 20 %, when the weight content of MWCNT is increased from 0 to 4 % within the epoxy matrix.
- The fracture energy and fracture toughness of the subsequent nanocomposite improved when the weight content of SWCNT and MWCNT is increased from 0 to 4 % within the epoxy matrix. The fracture energy is increased by 132 % and 237 % when the weight content of SWCNT and MWCNT is increased from 0 to 4 % within the epoxy matrix respectively.
- The fracture toughness increased by 169 % and 101 % when the weight content of SWCNT and MWCNT is increased from 0 to 4 % within the epoxy matrix respectively.
- The effect of aspect ratio on the fracture energy and fracture toughness of subsequent nanocomposite is also investigated for different SWCNT and MWCNT content in the epoxy matrix. The aspect ratio of SWCNT and MWCNT is varied in range of 200 to 1000 within

the matrix. Fracture energy and fracture toughness of the nanocomposite improved with the increase in aspect ratio of SWCNT and MWCNT within the epoxy matrix.

- From the crack growth simulations in polymer nanocomposite plate containing an edge and centre crack, the following salient points are concluded:
  - The failure crack length of an edge and centre cracked plate is 7 mm and 14 mm, when the 0 % CNT by weight is taken for numerical simulation respectively.
  - The failure crack length of an edge cracked plate is 27 mm and 19 mm, when the weight content of SWCNT and MWCNT is 4 % in the polymer nanocomposite respectively.
  - The failure crack length of a centre cracked plate is 66 mm and 50 mm, when the weight content of SWCNT and MWCNT is 4 % in the polymer nanocomposite respectively.
- SWCNT produces more pronounced effect on the failure crack length in comparison to MWCNT.

5.1 Scope for Future Work

Based on a number of previous researches, it has been well established that mechanical and fatigue performance of the epoxy resins can be enhanced by reinforcing CNTs. Despite the huge amount of work that has been done in the development of nanocomposites, there are still many challenges in processing these nanocomposites. Estimating the life of these novel materials is an important area of study which generally accounts a number of defects within the material in the form of cracks, voids and inclusions. In the present work, XFEM has been successfully utilized for modelling different crack conditions in a thin plate made up of CNT reinforced epoxy nanocomposite. But apart from cracks, a number of additional defects can be present in a material in the form of voids and inclusions. Presence of voids and inclusions can also have a significant impact on the life of the material. Since modelling of voids and inclusions is possible with XFEM, present work can be extended to model voids and inclusions within polymer nanocomposites. Furthermore, present work can also be extended to model a number of different other types of arbitrary crack conditions within the material. Modelling crack in a 3D space is also a possible future scenario.

References

[1] F. Hussain, M. Hojjati, M. Okamoto and R. Gorga, "Review article: polymer-matrix nanocomposites, processing, manufacturing, and application: an overview.," *Journal of composite materials,* vol. 40, no. 17, pp. 1511-1575, 2006.

[2] N. Domun, H. Hadavinia, T. Zhang, T. Sainsbury, G. Liaghat and S. Vahid, "Improving the fracture toughness and the strength of epoxy using nanomaterials–a review of the current status," *Nanoscale,* vol. 7, no. 23, pp. 10294-10329, 2015.

[3] S. Iijima, "Helical microtubules of graphitic carbon," *Nature,* vol. 354, pp. 56-58, 1991.

[4] R. Baughman, A. Zakhidov and W. De Heer, "Carbon nanotubes - the route toward applications," *Science,* vol. 297, no. 5582, pp. 787-792, 2002.

[5] J. Wilder, L. Rinzler, R. Smalley and C. Dekker, "Electronic structure of atomically resolved carbon nanotubes," *Nature,* vol. 391, no. 6662, pp. 59-62, 1998.

[6] M. Yu, O. Lourie, M. Dyer, K. Molony, T. Kelly and R. Ruoff, "Strength and breaking mechanism of multiwalled carbon nanotubes under tensile load," *Science,* vol. 287, no. 5453, pp. 637-640, 2000.

[7] O. Breuer and U. Sundararaj, "Big returns from small fibers: a review of polymer/carbon nanotube composites.," *Polymer composites,* vol. 25, no. 6, pp. 630-645, 2004.

[8] N. Tai, M. Yeh and T. Peng, "Experimental study and theoretical analysis on the mechanical properties of SWNTs/phenolic composites," *Composites: Part B,* vol. 39, p. 926–93, 2008.

[9] F. Gojny, M. Wichmann, B. Fiedler and K. Schulte, "Influence of different carbon nanotubes on the mechanical properties of epoxy matrix–a comparative study," *Composites Science and Technology,* vol. 65, no. 15, pp. 2300-2313, 2005.

[10] F. Gojny and K. Schulte, "Functionalisation effect on the thermo mechanical behaviour of multi-wall carbon nanotube/epoxy composites," *Composites Science and Technology,* vol. 64, no. 15, pp. 2303-2308, 2004.

[11] T. Hsieh, A. Kinloch, A. Taylor and I. Kinloch, "The effect of carbon nanotubes on the fracture toughness and fatigue performance of a thermosetting epoxy polymer," *Journal of Materials Science,* vol. 46, no. 23, p. 7525, 2011.

[12] W. Zhang, R. Picu and N. Koratkar, “The effect of carbon nanotube dimensions and dispersion on the fatigue behavior of epoxy nanocomposites,” *Nanotechnology,* vol. 19, no. 28, p. 285709, 2008.

[13] L. Tang, H. Zhang, J. Han, X. Wu and Z. Zhang, “Fracture mechanisms of epoxy filled with ozone functionalized multi-wall carbon nanotubes,” *Composite Science and Technology,* vol. 72, pp. 7-13, 2011.

[14] R. Ladani, S. Wu, A. Kinloch, K. Ghorbani, J. Zhang, A. Mouritz and C. Wang, “Improving the toughness and electrical conductivity of epoxy nanocomposites by using aligned carbon nanofibres,” *Composites Science and Technology,* vol. 117, pp. 146-158, 2015.

[15] T. Belytschko, Y. Lu and L. Gu, “Element-free Galerkin methods,” *International journal for numerical methods in engineering,* vol. 37, no. 2, pp. 229-256, 1994.

[16] W. Liu, S. Jun and Y. Zhang, “Reproducing kernel particle methods,” *International journal for numerical methods in fluids,* vol. 20, no. 8-9, pp. 1081-1106, 1995.

[17] S. Atluri and T. Zhu, “A new meshless local Petrov-Galerkin (MLPG) approach in computational mechanics,” *Computational mechanics,* vol. 22, no. 2, pp. 117-127, 1999.

[18] T. Belytschko and T. Black, “Elastic crack growth in finite elements with minimal remeshing,” *International journal for numerical methods in engineering,* vol. 45, no. 5, pp. 601-620, 1999.

[19] T. Hughes, J. Cottrell and Y. Bazilevs, “Isogeometric analysis: CAD, finite elements, NURBS, exact geometry and mesh refinement,” *Computer methods in applied mechanics and engineering,* vol. 194, no. 39, pp. 4135-4195, 2005.

[20] S. Mohammadi, Extended finite element method: for fracture analysis of structures, John Wiley & Sons, 2008.

[21] S. Osher and J. Sethian, “Fronts propagating with curvature-dependent speed: algorithms based on Hamilton-Jacobi formulations,” *Journal of computational physics,* vol. 79, no. 1, pp. 12-49, 1988.

[22] M. Stolarska, D. Chopp, N. Moës and T. Belytschko, “Modelling crack growth by level sets in the extended finite element method,” *International journal for numerical methods in Engineering,* vol. 51, no. 8, pp. 943-960, 2001.

[23] N. Sukumar, D. Chopp, N. Moës and T. Belytschko, "Modeling holes and inclusions by level sets in the extended finite-element method," *Computer methods in applied mechanics and engineering,* vol. 190, no. 46, pp. 6183-6200, 2001.

[24] C. Daux, N. Moes, J. Dolbow, N. Sukumar and T. Belytschko, "Arbitrary branched and intersecting cracks with the extended finite element method," *Int. J. Numer. Meth. Eng,* vol. 48, p. 1741–1760, 2000.

[25] N. Sukumar and J. Prévost, "Modeling quasi-static crack growth with the extended finite element method Part I: Computer implementation," *International journal of solids and structures,* vol. 40, no. 26, pp. 7513-7537, 2003.

[26] E. Wyart, M. Duflot, D. Coulon, P. Martiny, T. Pardoen, J. Remacle and F. Lani, "Substructuring FE–XFE approaches applied to three-dimensional crack propagation," *Journal of Computational and Applied Mathematics,* vol. 215, no. 2, pp. 626-638, 2008.

[27] E. Wong, P. Sheehan and C. Lieber, "Nanobeam mechanics: elasticity, strength, and toughness of nanorods and nanotubes," *Science,* p. 1971–1975, 1997.

[28] K. Awasthi, A. Srivastava and O. Srivastava, "Synthesis of carbon nanotubes," *Journal of nanoscience and nanotechnology,* vol. 5, no. 10, pp. 1616-1636, 2005.

[29] K. Hata, D. N. Futaba, K. Mizuno, T. Namai, M. Yumura and S. Iijima, "Water-assisted highly efficient synthesis of impurity-free single-walled carbon nanotubes," *Science,* vol. 306, no. 5700, p. 1362–1364, 2004.

[30] D. S. Bethune, C. H. Klang, M. S. De Vries, G. Gorman, R. Savoy, J. Vazquez and R. Beyers, "Cobalt-catalysed growth of carbon nanotubes with single-atomic-layer walls," *Nature,* vol. 363, no. 6430, pp. 605-607, 1993.

[31] S. Iijima and T. Ichihashi, "Single-shell carbon nanotubes of 1-nm diameter," *Nature,* vol. 363, no. 6430, pp. 603-605, 1993.

[32] M. Monthioux, "Filling single-wall carbon nanotubes," *Carbon,* vol. 40, pp. 1809-1823, 2002.

[33] M. Dresselhaus, G. Dresselhaus and P. Avouris, Carbon nanotubes: synthesis, structure, properties, and applications (Vol. 80), Springer Science & Business Media, 2003.

[34] E. Thostenson, R. Zhifeng and T. Chou, "Advances in the science and technology of carbon nanotubes and their composites: a review," *Composites science and technology,* vol. 61, no. 13, pp. 1899-1912, 2001.

[35] S. Reich, . C. Thomsen and J. Maultzsch, Carbon nanotubes: basic concepts and physical properties, John Wiley & Son, 2008.

[36] K. Balasubramanian and M. Burghard, "Chemically functionalized carbon nanotubes," *Small,* vol. 1, no. 2, pp. 180-192, 2005.

[37] . B. T. Kelly, Physics of graphite, London: Applied Science, 1981.

[38] M. Treacy, T. Ebbesen and J. Gibson, "Exceptionally high Young's modulus observed for individual carbon nanotubes," *Nature,* vol. 381, no. 6584, p. 678–680, 1996.

[39] P. Poncharal, Z. Wang, D. Ugarte and W. Heer, "Electrostatic deflections and electromechanical resonances of carbon nanotubes," *Science,* vol. 283, no. 5407, p. 1513–1516, 1999.

[40] J. P. Salvetat, A. J. Kulik, J. M. Bonard, G. A. D. Briggs, T. Stöckli, . K. Méténier and L. Forró, "Elastic modulus of ordered and disordered multiwalled carbon nanotubes," *Advanced Materials,* vol. 11, no. 2, pp. 161-165, 1999.

[41] . N. Behabtu, C. C. Young, D. E. Tsentalovich, O. Kleinerman, X. Wang, A. W. Ma and S. B. Fairchild, "Strong, light, multifunctional fibers of carbon nanotubes with ultrahigh conductivity," *Science,* vol. 339, no. 6116, pp. 182-186, 2013.

[42] J. P. Salvetat, G. A. D. Briggs, J. M. Bonard, R. R. Bacsa, A. J. Kulik, T. Stöckli and L. Forró, "Elastic and shear moduli of single-walled carbon nanotube ropes," *Physical review letters,* vol. 82, no. 5, p. 944, 1999.

[43] M. Yu, B. Files, . S. Arepalli and R. Ruoff, "Tensile loading of ropes of single wall carbon nanotubes and their mechanical properties," *Physical review letters,* vol. 84, no. 24, p. 5552, 2000.

[44] A. Lau and D. Hui, "The revolutionary creation of new advanced materials—carbon nanotube composites," *Composites Part B: Engineering,* vol. 33, no. 4, pp. 263-277, 2002.

[45] B. Vigolo, A. Penicaud, C. Coulon, . C. Sauder, R. Pailler, C. Journet and . P. Poulin, "Macroscopic fibers and ribbons of oriented carbon nanotubes," *Science,* vol. 290, no. 5495, pp. 1331-1334, 2000.

[46] D. Hull and . T. W. Clyne, An introduction to composite materials, Cambridge University press, 1996.

[47] R. e. Shalin, Polymer matrix composites (Vol. 4), Springer Science & Business Media, 2012.

[48] L. McAdams and J. Gannon, "Epoxy resins," in *High performance polymers and composites*, Polymers Encyclopedia Reprint Series, John Wiley & Sons, 1991, pp. 258-318.

[49] T. Ueki, S. Nishijima and Y. Izumi, "Designing of epoxy resin systems for cryogenic use," *Cryogenics*, vol. 45, no. 2, pp. 141-148, 2005.

[50] L. C. Tang, X. Wang, Y. J. Wan, L. B. Wu, J. X. Jiang and G. Q. Lai, "Mechanical Properties and fracture behaviors of epoxy composites with multi-scale rubber particles," *Materials Chemistry and Physics*, vol. 141, no. 1, pp. 333-342, 2013.

[51] C. Inglis, "Stresses in a cracked plate due to the presence of cracks and sharp corners," *Trans Nav Archit (London)*, no. 60, p. 213, 1913.

[52] A. Griffith, "The phenomena of rupture and flow in solids," *Philosophical transactions of the royal society of london. Series A, containing papers of a mathematical or physical character*, no. 221, pp. 163-198, 1921.

[53] T. Anderson, Fracture mechanics: fundamentals and applications, CRC press, 2005.

[54] M. L. Manchado, L. Valentini, J. Biagiotti and J. M. Kenny, "Thermal and mechanical properties of single-walled carbon nanotubes–polypropylene composites prepared by melt processing," *Carbon*, vol. 43, no. 7, pp. 1499-1505, 2005.

[55] X. Xie, Y. Mai and X. Zhou, "Dispersion and alignment of carbon nanotubes in polymer matrix: a review," *Materials Science and Engineering: R: Reports*, vol. 49, no. 4, pp. 89-112, 2005.

[56] E. T. Thostenson and T. Chou, "Processing structure multi-functional property relationship in carbon nanotube/epoxy composites," *Carbon*, vol. 44, no. 14, pp. 3022-3029, 2006.

[57] Y. Song and J. Youn, "Influence of dispersion states of carbon nanotubes on physical properties of epoxy nanocomposites," *Carbon*, vol. 43, no. 7, pp. 1378-1385, 2005.

[58] . S. U. Khan, J. R. Pothnis and J. K. Kim, "Effects of carbon nanotube alignment on electrical and mechanical properties of epoxy nanocomposites,," *Composites Part A: Applied Science and Manufacturing*, vol. 49, pp. 26-34, 2013.

[59] Q. Wang, J. Dai, W. Li, Z. Wei and J. Jiang, "The effects of CNT alignment on electrical conductivity and mechanical properties of SWNT/epoxy nanocomposites," *Composites science and technology,* vol. 68, no. 7, pp. 1644-1648, 2008.

[60] P. M. Ajayan, O. Stephan, C. Colliex and D. Trauth, "Aligned carbon nanotube arrays formed by cutting a polymer resin-nanotube composite," *Science-AAAS-Weekly Paper Edition,* vol. 265, no. 5176, pp. 1212-1214, 1994.

[61] S. J. V. Frankland, A. Caglar, D. W. Brenner and M. Griebel, "Molecular simulation of the influence of chemical cross-links on the shear strength of carbon nanotube− polymer interfaces," *The Journal of Physical Chemistry B,* vol. 106, no. 12, pp. 3046-3048, 2002.

[62] P. Ma, J. Kim and B. Tang, "Effects of silane functionalization on the properties of carbon nanotube/epoxy nanocomposites," *Composites Science and Technology,* vol. 67, no. 14, pp. 2965-2972, 2007.

[63] L. Sun, G. Warren, J. O'reilly, W. Everett, S. Lee, D. Davis, D. Lagoudas and H. Sue, "Mechanical properties of surface-functionalized SWCNT/epoxy composites," *Carbon,* vol. 46, no. 2, pp. 320-328, 2008.

[64] M. Quaresimin, K. Schulte, M. Zappalorto and S. Chandrasekaran, "Toughening mechanisms in polymer nanocomposites: From experiments to modelling," *Composites Science and Technology,* vol. 123, pp. 187-204, 2016.

[65] T. H. Hsieh, A. J. Kinloch, A. C. Taylor and S. Sprenger, "The Effect of Silica Nanoparticles and Carbon Nanotubes on the Toughness of a Thermosetting Epoxy Polymer," *Journal of Materials Science,* vol. 119, no. 4, p. 2135–2142, 2011.

[66] M. Ayatollahi, S. Shadlou and M. Shokrieh, "Fracture toughness of epoxy/multi-walled carbon nanotube nano-composites under bending and shear loading conditions," *Materials & Design,* vol. 32, no. 4, pp. 2115-2124, 2011.

[67] M. Ayatollahi, S. Shadlou and M. Shokrieh, "Mixed mode brittle fracture in epoxy/multi-walled carbon nanotube nanocomposites," *Engineering Fracture Mechanics,* vol. 78, no. 14, pp. 2620-2632, 2011.

[68] J. Yang, Z. Chen, Q. Feng, Y. Deng, Y. Liu, Q. Ni and S. Fu, "Cryogenic mechanical behaviors of carbon nanotube reinforced composites based on modified epoxy by poly (ethersulfone)," *Composites Part B: Engineering,* vol. 43, no. 1, pp. 22-26, 2012.

[69] Z. Chen, J. Yang, Q. Ni, S. Fu and Y. Huang, "Reinforcement of epoxy resins with multi-walled carbon nanotubes for enhancing cryogenic mechanical properties," *Polymer*, vol. 50, no. 19, pp. 4753-4759, 2009.

[70] J. Halpin, Primer on Composite Materials Analysis (Revised), CRC Press, 1992.

[71] J. Halpin, "Stiffness and expansion estimates for oriented short fiber composites," *Journal of Composite Materials,* vol. 3, no. 4, pp. 732-734, 1969.

[72] E. Thostenson and T. Chou, "On the elastic properties of carbon nanotube-based composites: modelling and characterization," *Journal of Physics D: Applied Physics,* vol. 36, no. 5, p. 573, 2003.

[73] J. Blanco, E. García, R. de Villoria and B. Wardle, "Limiting mechanisms of mode I interlaminar toughening of composites reinforced with aligned carbon nanotubes," *Journal of Composite Materials,* vol. 43, no. 8, pp. 825-841, 2009.

[74] A. Barber, S. Cohen and H. Wagner, "Measurement of carbon nanotube–polymer interfacial strength," *Applied Physics Letters,* vol. 82, no. 23, pp. 4140-4142, 2003.

[75] A. Kelly and A. Tyson, "Tensile properties of fibre-reinforced metals: copper/tungsten and copper/molybdenum," *Journal of the Mechanics and Physics of Solids,* vol. 13, no. 6, pp. 1339-338, 1965.

[76] V. Mirjalili and P. Hubert, "Modelling of the carbon nanotube bridging effect on the toughening of polymers and experimental verification," *Composites Science and Technology,* vol. 70, no. 10, pp. 1537-1543, 2010.

[77] J. Dolbow and . T. Belytschko, "A finite element method for crack growth without remeshing," *International journal for numerical methods in engineering,* vol. 46, no. 1, pp. 131-150, 1999.

[78] I. Singh, B. Mishra, S. Bhattacharya and R. Patil, "The numerical simulation of fatigue crack growth using extended finite element method," *International Journal of Fatigue,* vol. 36, no. 1, pp. 109-119, 2012.

[79] B. Rao and S. Rahman, "A new interaction integral method for analysis of cracks in orthotropic functionally graded materials," in *ASME 2003 Pressure Vessels and Piping Conference*, 2003.

[80] F. Li, C. Shih and A. Needleman, "A comparison of methods for calculating energy release rates," *Engineering Fracture Mechanics,* vol. 21, no. 2, pp. 405-421, 1985.

[81] J. Dolbow and T. Belytschko, “A finite element method for crack growth without remeshing,” *International journal for numerical methods in engineering,* vol. 46, no. 1, pp. 131-150, 1999.

[82] N. Domun, H. Hadavinia, T. Zhang, T. Sainsbury, G. Liaghat and S. Vahid, “Improving the fracture toughness and the strength of epoxy using nanomaterials–a review of the current status,” *Nanoscale,* vol. 7, no. 23, pp. 10294-10329, 2015.

[83] S. Xie, W. Li, Z. Pan, B. Chang and L. Sun, “Mechanical and physical properties on carbon nanotube,” *Journal of Physics and Chemistry of solids,* vol. 61, no. 7, pp. 1153-1158, 2000.

Web References

W1.	Nanoshel LLC	https://www.nanoshel.com/multi-walled-carbon-nanotubes (accessed on 25/05/2017)
W2.	TASC-Single Wall CNT	http://www.tasc-nt.or.jp/en/project/characteristic.html (accessed on 25/05/2017)

Appendix A

Equivalent Properties of CNT reinforced Polymer Nanocomposite

Table A.1: Equivalent properties of SWCNT reinforced epoxy nanocomposite

CNTs wt. %	CNTs volume %	Elastic Modulus (GPa)	Poisson's Ratio	Fracture Energy (J/m^2)	Fracture Toughness ($MPa\ m^{1/2}$)
0	0.0000	2.9000	0.3500	133.0000	0.6210
0.5	0.3339	3.6441	0.3494	154.7809	0.7510
1	0.6689	4.3930	0.3487	176.6347	0.8809
1.5	1.0050	5.1465	0.3481	198.5617	1.0109
2	1.3423	5.9047	0.3474	220.5622	1.1412
2.5	1.6807	6.6678	0.3468	242.6368	1.2720
3	2.0202	7.4357	0.3462	264.7856	1.4032
3.5	2.3609	8.2085	0.3455	287.0091	1.5349
4	2.7027	8.9863	0.3449	309.3078	1.6672

Table A.2: Equivalent properties of MWCNT reinforced epoxy nanocomposite

CNTs wt. %	CNTs volume %	Elastic Modulus (GPa)	Poisson's Ratio	Fracture Energy (J/m^2)	Fracture Toughness ($MPa\ m^{1/2}$)
0	0.0000	2.9000	0.3500	133.0000	0.6210
0.5	0.3339	2.9714	0.3494	171.8811	0.7146
1	0.6689	3.0431	0.3487	210.8922	0.8011
1.5	1.0050	3.1152	0.3481	250.0339	0.8826
2	1.3423	3.1876	0.3474	289.3071	0.9603
2.5	1.6807	3.2603	0.3468	328.7122	1.0352
3	2.0202	3.3334	0.3462	368.2500	1.1079
3.5	2.3609	3.4069	0.3455	407.9212	1.1789
4	2.7027	3.4807	0.3449	447.7264	1.2484

Appendix B

Key Simulation Results

Table B.1: SIF value for SWCNT reinforced nanocomposite plate containing an edge crack

	Stress Intensity Factors (MPa mm$^{1/2}$)				
Crack length (mm)	**0 % CNT**	**1 % CNT**	**2 % CNT**	**3 % CNT**	**4 % CNT**
5	15.88700	15.88709	15.88719	15.88729	15.88738
7	19.47913	19.47911	19.47910	19.47908	19.47906
9		22.59339	22.59335	22.59331	22.59327
11		25.55825	25.55823	25.55821	25.55819
13			28.52739	28.52739	28.52740
15			31.42435	31.42441	31.42447
17			34.44508	34.44498	34.44487
19				37.57553	37.57545
21				40.92645	40.92642
23					44.60677
25					48.06013
27					51.90390

Table B.2: SIF values for MWCNT reinforced nanocomposite plate containing an edge crack

	Stress Intensity Factors (MPa mm$^{1/2}$)				
Crack length (mm)	**0 % CNT**	**1 % CNT**	**2 % CNT**	**3 % CNT**	**4 % CNT**
5	15.88700	15.88709	15.88719	15.88729	15.88738
7	19.47913	19.47911	19.47910	19.47908	19.47906
9		22.59339	22.59335	22.59331	22.59327
11			25.55823	25.55821	25.55819
13			28.52739	28.52739	28.52740
15				31.42441	31.42447
17				34.44498	34.44487
19					37.57545

Table B.3: SIF values for SWCNT reinforced nanocomposite plate containing a centre crack

	Stress Intensity Factors (MPa mm$^{1/2}$)				
Crack length (mm)	**0 % CNT**	**1 % CNT**	**2 % CNT**	**3 % CNT**	**4 % CNT**
10	14.74695	14.74698	14.74700	14.74703	14.74705
14	17.73639	17.73649	17.73659	17.73669	17.73679
18		19.88319	19.88318	19.88318	19.88317
22		22.25628	22.25661	22.25695	22.25728
26		24.19242	24.19259	24.19276	24.19293
30		26.38850	26.38857	26.38864	26.38870
34			28.59222	28.59225	28.59229
38			30.85064	30.85072	30.85080
42			33.13689	33.13690	33.13691
46			35.57718	35.57718	35.57717
50				38.20426	38.20426
54				41.12429	41.12433
58				44.11355	44.11358
62					47.71931
66					51.75086

Table B.4: SIF values for MWCNT reinforced nanocomposite plate containing a centre crack

	Stress Intensity Factors (MPa mm$^{1/2}$)				
Crack length (mm)	**0 % CNT**	**1 % CNT**	**2 % CNT**	**3 % CNT**	**4 % CNT**
10	14.74695	14.74698	14.74700	14.74703	14.74705
14	17.73639	17.73649	17.73659	17.73669	17.73679
18		19.88319	19.88318	19.88318	19.88317
22		22.25628	22.25661	22.25695	22.25728
26		24.19242	24.19259	24.19276	24.19293
30			26.38857	26.38864	26.38870
34			28.59222	28.59225	28.59229
38				30.85072	30.85080

42				33.13690	33.13691
46					35.57717
50					38.20426

Alok_13-07-2017

ORIGINALITY REPORT

%11	%1	%11	%2
SIMILARITY INDEX	INTERNET SOURCES	PUBLICATIONS	STUDENT PAPERS

PRIMARY SOURCES

1	Handbook of Polymer Nanocomposites Processing Performance and Application, 2015. Publication	%1
2	Kumar, Sachin, I.V. Singh, and B.K. Mishra. "A homogenized XFEM approach to simulate fatigue crack growth problems", Computers & Structures, 2015. Publication	%1
3	T. H. Hsieh. "The effect of carbon nanotubes on the fracture toughness and fatigue performance of a thermosetting epoxy polymer", Journal of Materials Science, 06/29/2011 Publication	%1
4	Mohammadi, . "Extended Finite Element Method", XFEM Fracture Analysis of Composites Mohammadi/XFEM Fracture Analysis of Composites, 2012. Publication	%1
5	Fracture of Engineering Materials and	%1